

A three-dimensional implementation of the boundary element and level set based structural optimisation

B.Ullah*, J.Trevelyan, I.Ivrissimtzis

*School of Engineering and Computing Sciences, Durham University,
South Road, Durham DH1 3LE, UK.*

Abstract

This paper presents a three-dimensional structural optimisation approach based on the boundary element and level set methods. The structural geometry is implicitly represented with the level set method, which evolves an initial structural model towards an optimal configuration using an evolutionary structural optimisation approach. The boundary movements in the three-dimensional level set based optimisation method allow automatic hole nucleation through the intersection of two surfaces moving towards each other. This suggests that perturbing only the boundary can give rise to changes not only in shape, but also in topology. At each optimisation iteration, the Marching Cubes algorithm is used to extract the modified geometry (i.e. the zero level set contours) in the form of a triangular mesh. As the boundary element method is based on a boundary discretisation approach, the extracted geometry (in the form of a triangular mesh) can be directly analysed within it. However, some mesh smoothing is required; HC-Laplacian smoothing is a useful algorithm that overcomes the volumetric loss associated with simpler algorithms. This eliminates the need for an additional discretisation tool and provides a natural link between the implicitly represented geometry and its structural model throughout the optimisation process. A complete algorithm is proposed and tested for the boundary element and level set methods based topology optimisation in three-dimensions. Optimal geometries compare well against those in the literature for a range of benchmark examples.

Keywords: structural optimisation, boundary element method, level set

*Corresponding author

Email address: baseerullah@gmail.com (B.Ullah)

1. Introduction

The level set method (LSM) is an efficient numerical technique originally developed by Osher and Sethian [1] for the tracking of propagating interfaces with natural adaptation to topological changes such as merging and breaking. There is a wide variety of applications, including structural optimisation, in which the LSM has been successfully employed. Sethian and Wiegmann [2] first presented a level set (LS) based structural optimisation method, where shape and topological changes were accomplished through a von Mises stress based criterion. Osher and Santosa [3] proposed a LS based method using shape sensitivity analysis for the optimisation of an inhomogeneous drum for the frequency response. Wang *et al.* [4] proposed a shape sensitivity approach for the solution of minimum compliance problems. Allaire *et al.* [5] independently proposed a LS based optimisation method based on shape sensitivities for the solution of two and three-dimensional optimisation problems with both linear and non-linear structural material.

In the LS based optimisation approaches, the selection of an effective structural performance measuring tool, and an efficient optimisation technique play an important role for the solution of the optimisation problems. The performance measuring tool evaluates the structural response against the applied load and boundary conditions. These responses are then converted into a useful form by the optimisation technique, which evolves the structural geometry accordingly. The performance of a candidate design can be measured through a geometry mapping technique, which projects the implicitly represented geometry onto the structural model. The most commonly used geometry mapping techniques in the LS based structural optimisation are material distribution (density based), immersed boundary and conforming discretisation [6].

Most of the LS based optimisation methods utilise a fixed Eulerian type mesh with an “Ersatz material” approach [5] as an alternative finite element (FE) analysis tool. The structural geometry is represented through a density distribution function, i.e. ($\eta < \rho < 1$), similar to the density based optimisation approach [7]. Solid material is represented by ($\rho = 1$) and holes in the structure are replaced by a specified minimum relative density ($\rho = \eta$). Wang *et al.* [4] and Allaire *et al.* [5] initially implemented the density based

approaches in their proposed LS based topology optimisation methods. Although the fixed grid is a simple approach, it is not effective to capture the exact geometry of the boundary [5] and a highly dense grid distribution is always required near the boundary for high accuracy [8]. In addition, the presence of intermediate material densities along the structural boundary can result in indistinct boundary representation [9], which can cause uncertainty when transferring the optimum design to manufacture. A smoothed Heaviside function approach has been adopted to smooth the discontinuity at the boundary [10, 11]. However, the numerical integration of the stiffness matrix may be less accurate [12].

The immersed boundary approach uses a non body conforming fixed grid, where the structural geometry is not aligned with the Eulerian grid and can intersect some grid cells. This approach allows a clear boundary representation and avoids intermediate density material [6]. Sethian and Wiegmann [2] used the immersed interface method within a finite difference framework for the solution of the LS based topology optimisation problems. The extended finite element method (X-FEM) can also be used to evaluate the structural response at the design boundary through the local enrichment of elements intersected by the zero level set contour [13]. Belytschko *et al.* [14] combined the implicit boundary representation with the X-FEM approach for the solution of topology optimisation problems. Further implementations of the X-FEM within a level set framework can be found in [15, 16]. Yamasaki *et al.* [9] developed a two-dimensional topology optimisation method for minimum compliance problems based on the immersed boundary mapping, boundary element and level set methods. The common problem reported in the implementation of the immersed boundary methods is the occurrence of small intersection of finite elements [15] or short boundary elements [9] while discretising the structural model. This can profoundly affect the accuracy of the structural response. Further, the use of immersed boundary techniques requires sophisticated codes and can make their implementation difficult and time consuming [6].

In contrast to the density and immersed boundary mapping, some of the LS based optimisation methods use two types of discretisation during the numerical implementation, i.e. a fixed Eulerian discretisation which maintains the LS function throughout the optimisation process, and a body conforming discretisation which exactly fits the design domain. Two different approaches can be used to discretise the design domain; the FEM based domain discretisation, and the boundary element method (BEM) based boundary only

discretisation. The body conforming discretisation provides the most accurate analysis of the structural model, especially along the boundary. Ha and Cho [17] utilised an unstructured conforming discretisation approach for the optimisation of geometrically nonlinear structures within the LS framework. Yamasaki *et al.* [18] presented a boundary tracking approach for the LS based topology optimisation using a conforming discretisation approach and geometry based re-initialisation scheme [19]. The use of BEM for the solution of minimum compliance problems within a two-dimensional LSM based optimisation method was first proposed by Abe *et al.* [20]. Later on, the proposed approach has also been extended for shape optimisation related to sound scattering problems [21].

In comparison with the immersed boundary mapping, the body conforming approach is attractive due to its simplicity and higher accuracy. A FEM based body conforming mapping may require special care to mesh a two-dimensional geometry and can make the discretisation of a three-dimensional arbitrary geometry more complicated and time consuming. As a consequence it could be difficult to ensure the analysis accuracy for a continuously changing finite element model. In contrast, the BEM based body conforming mapping is very attractive because it requires discretisation only at the design boundary, i.e. directly along the zero level set contours and significantly decreases the degrees of freedom in comparison with the FEM. This reduction of problem dimensionality simplifies considerably the re-meshing task (especially in three-dimensions), which can be performed efficiently and robustly. Thus, its rapid and robust re-meshing and accurate boundary solutions make the boundary based body mapping method a natural choice for the solution of the LS based shape and topology optimisation problems.

In a LS based optimisation method, an improvement in the design is mainly governed by changes in its shape. These changes can be carried out either with shape sensitivity information (e.g. [3, 4, 22, 23, 24]) or through an evolutionary approach based on the von Mises stress criterion (e.g. [2]). The sensitivity based techniques are popular because they are efficient although they require the computation of suitably accurate gradients, which may not be available. Moreover, these methods can often have difficulties in dealing with local optima. They are complex algorithms that are difficult to implement efficiently. Compared to the shape sensitivity approach, the evolutionary structural optimisation (ESO) methods are simple to implement, robust, and capable of dealing with almost any kind of structural optimisation problem, see for example [25]. The ESO schemes have remained popular

on account of their simplicity and extensive empirical evidence of the fact that their optimal solutions closely resemble those derived by more rigorous descent methods (e.g. Li *et al.* [26]).

The use of ESO in a BEM and LSM based optimisation method has been first investigated in [27, 28] for the solution of two dimensional optimisation problems. The implementation of a hole insertion mechanism in those studies provides optimal configurations insensitive to initial designs. However, the computation of the structural response at points inside the design domain is necessary to find the optimal locations for new hole insertions, and a direct extension of the proposed approach to three-dimensions would require additional efforts to calculate the structural response within the design domain. Instead, the boundary movements in a three-dimensional LS based optimisation method allow automatic hole nucleation through the intersection of two approaching surfaces [5], and consequently, the boundary only perturbation can give rise to changes not only in shape, but also in topology. Moreover, the BEM allows the evaluation of the structural response directly at the design boundary and its integration with the LSM, effectively handling shape and topology optimisation at the same time and eliminating the need for calculating the structural response within the design domain. This suggests a considerable reduction of the problem dimensionality in a three-dimensional implementation.

In a three-dimensional LS based optimisation approach, the structural geometry can be easily re-constructed in the form of a triangular surface mesh using a Marching Cubes (MC) algorithm. This allows automatic boundary discretisation of the modified structural geometry at each optimisation iteration. The accuracy and convergence of the boundary element analysis (BEA) for this discretised geometry can be further improved with mesh smoothing schemes, e.g. HC-Laplacian smoothing.

In the literature of LS based optimisation methods, the use of BEM is in the very early stages, and relatively few methods are available, e.g. [9, 20]. In addition, these methods are limited to the solution of two-dimensional problems. The boundary-only intrinsic characteristic of the BEM together with the LSM makes this combination especially attractive for solving optimisation problems in three-dimensions, and requires a comprehensive investigation to propose an effective and reliable methodology. Therefore, the goal of the research work presented in this paper is to propose an optimisation approach for efficient utilisation of the advantageous features resulting from the integration of BEM, LSM and ESO. The authors have demonstrated

this effective combination in two-dimensions [27, 28] and, the extension of these ideas to three-dimensions in the current work. In comparison with competing FE-based approaches, it benefits from more automation, more robust mapping between the geometric and analysis models and a reduction in dimensionality since internal stresses are not required.

This paper is organised as follows. In section 2, we discuss the three-dimensional LSM and ESO based structural optimisation approach. The proposed algorithm and its implementation details are presented in Section 3. In Section 3.6, the BEM is introduced. In section 4, we present numerical examples, and discuss the performance of the proposed optimisation method. The paper closes with some concluding remarks in Section 5.

2. Level set based three-dimensional structural optimisation

The use of the LSM in three-dimensional optimisation has several advantages. The first one is related to its natural extension from two to three-dimensional space [29]. Another important advantage is that the LSM efficiently handles shape and topology optimisation simultaneously through automatic hole nucleation by the intersection of two surfaces moving towards each other [5]. Therefore its integration with the BEM, where the structural response can be directly evaluated at the design boundary, eliminates the need for a volumetric mesh of the evolving structural geometry. This suggests that in comparison with the available optimisation approaches, the combination of the BEM and LSM is computationally more efficient for the solution of three-dimensional structural optimisation problems.

The proposed three-dimensional optimisation approach is based on a bi-directional evolutionary structural optimisation approach (BESO) [30]. The BESO approach is based on the von Mises stress criterion, which progressively removes inefficient material from the low stressed regions and adds efficient material to the high stressed regions of the structure. Therefore, in the current implementation a gradient free approach is used to link the response of the structural model with the normal velocity of the implicitly represented geometry for its evolution during the optimisation process. This selection is based on two main reasons: Firstly, Li *et al.* [26] suggested that in an ESO method the compliance minimisation problem can be solved by directly using the von Mises stress criterion, and vice versa. Secondly, in the current research work, material addition is based on the material yield stress (see Section 3.7) which is normally used as a failure indicator in structural design.

Therefore, it is quite appropriate to use the von Mises stress criterion directly, and the optimal designs so produced should be expected to correlate with those produced using compliance sensitivity criteria.

The propagation of the structural boundary during the optimisation process can be linked with the evolution of the function ϕ as an initial value problem. This means that the position of the structural boundary at any time t is given by the zero level set of the function ϕ . The structural boundary is evolved with the solution of the Hamilton-Jacobi (HJ) equation [1]

$$\frac{\partial\phi}{\partial t} + F|\nabla\phi| = 0 \quad (1)$$

where F is the velocity in the normal direction and t is the virtual time. The normal velocity along the boundary can be computed from the structural response, e.g shape sensitivity analysis ([4, 5]). However, in the current implementation a normal velocity field which describes the motion of a point on the boundary is constructed from the von Mises stress distribution [28], and the structural boundary is then propagated through the use of virtual time stepping.

3. Optimisation algorithm

The proposed optimisation algorithm is illustrated in Figure 1 and summarised as follows:

1. Define structural geometry with applied loads and constraints.
2. Initialise level set grid with signed distance function to represent structural geometry implicitly.
3. Use the Marching Cubes algorithm to extract the zero level contours in the form of a triangular mesh.
4. Perform mesh postprocessing and improvement.
5. Carry out boundary element analysis.
6. Compute velocity at each node point of the structural boundary using the BE analysis results.
7. Extend boundary velocities to level set grid points in the narrow band.
8. Solve Equation (1) to update the level set function.
9. Repeat the above procedure from step 3 to 8, until the stopping criterion is satisfied.

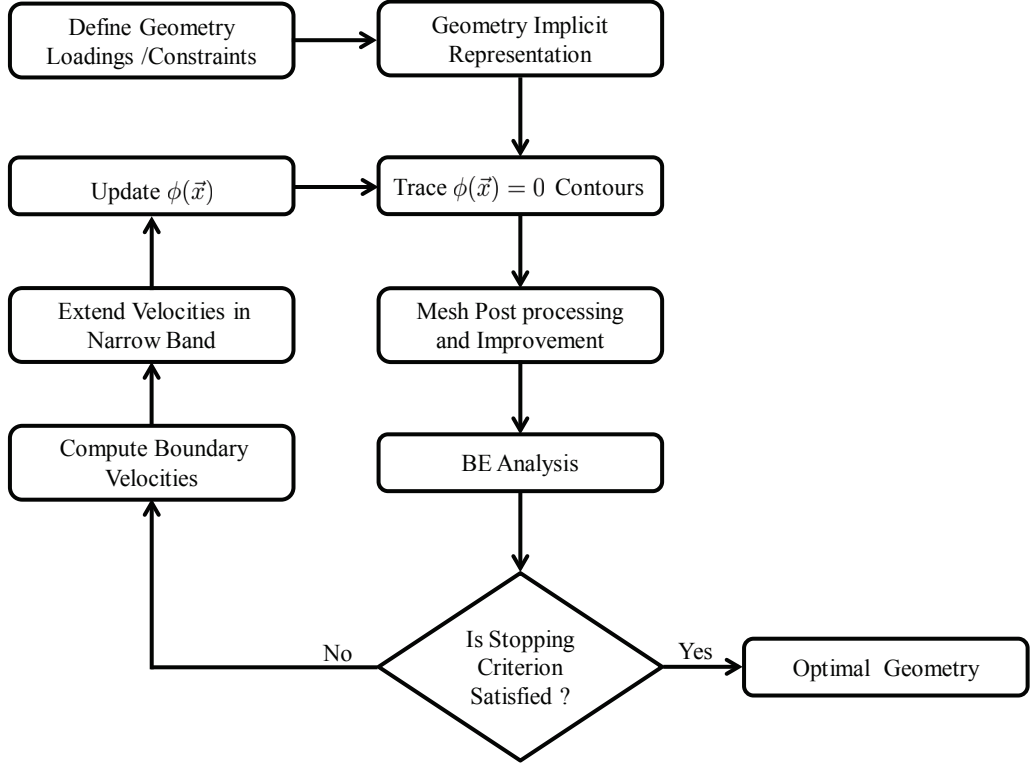


Figure 1: Optimisation flow chart

We start by defining our three-dimensional design domain $\Omega \subset \mathbb{R}^3$, having boundary Γ . In order to enhance the structural performance from both the stiffness and efficient material utilisation points of view the concept of specific stiffness was developed [31], being defined as,

$$f_K = \frac{K}{V} \quad (2)$$

where K is the stiffness and V is the volume of the structure. An equivalent concept in terms of the compliance is the specific strain energy, f_U , which is the product of strain energy U and the volume V of the structure [33], i.e.

$$f_U = UV \quad (3)$$

The expression used for strain energy calculation is,

$$U = \int_{\Gamma} \frac{1}{2} t_i u_i d\Gamma \quad (4)$$

where t_i is the traction and u_i is the displacement at a given node i . In practice, since the product $t_i u_i$ is non-zero only over elements on which a non-zero traction boundary condition has been prescribed (assuming there are no non-zero displacement constraints applied) the integral involved in Equation (4) conveniently reduces to the integral taken only over these elements.

The optimisation progress can be monitored using the reduction in f_U , and the target volume fraction can be used as a stopping criterion. The volume fraction α at a given stage of the optimisation process can be defined as,

$$\alpha = V/V_0 \quad (5)$$

where V is the volume at the current iteration and V_0 the initial volume of the structure.

The following sections discuss the implementation details of the various steps of the above optimisation algorithm.

3.1. Structural geometry, loading and constraints

The optimisation process starts with the definition of structural geometry, the applied loads and constraints. The geometry of this initial structure is arbitrary, and in most research work of this type, the initial geometry is a simple rectangular cuboid. The boundary Γ of the initial design domain Ω is decomposed into three parts,

$$\Gamma = \Gamma_0 \cup \Gamma_1 \cup \Gamma_2 \quad (6)$$

where Γ_0 corresponds to Dirichlet boundary conditions (where displacements are zeros), Γ_1 corresponds to non-homogeneous Neumann boundary conditions (where tractions are prescribed) and Γ_2 corresponds to homogeneous Neumann boundary conditions (which are traction-free and over which the geometry is allowed to change during the optimisation process).

3.2. Structural geometry implicit representation

The LSM uses the Eulerian approach to represent an evolving geometry implicitly. In a LS based structural optimisation, the structural geometry is first embedded as the zero level set of a higher dimensional function ϕ . A rectangular level set domain Ω_L with dimensions slightly bigger than the initial design domain Ω is used to capture all the possible geometry changes during the optimisation process. In most cases, the initial function ϕ is defined as the distance of a particular grid point from the boundary with a sign

to indicate points either inside or outside of the boundary. Mathematically, it can be written as,

$$\phi(\vec{x}) \begin{cases} < 0 & \vec{x} \in \Omega \\ = 0 & \vec{x} \in \partial\Omega \text{ or } \Gamma \\ > 0 & \vec{x} \notin \Omega \end{cases} \quad (7)$$

where $\partial\Omega$ represents the zero level set contour.

Based on the proposed optimisation algorithm, a structural model of the implicitly represented geometry is always required at each optimisation iteration to measure its response against the applied loads and to evolve the design boundary accordingly. Therefore, after the initialisation of the level set grid and each update of the level set function (during the optimisation process), the structural geometry needs to be reconstructed from the three-dimensional level set grid using an efficient contour tracing algorithm. The implementation details of the contour tracing algorithm used in this study are presented in the following section.

3.3. Algorithm for tracing the zero level set contours

In the literature there are various approaches to the surface generation problems [34]. Due to its simplicity, efficiency and robustness, the MC algorithm is the most popular for extracting iso-surfaces from implicit functions. It has been widely studied, improved, and extended. The initial MC algorithm described by Lorensen and Cline [35] constructs a piecewise linear approximation of the level set $\{\vec{x}(x, y, z) : \phi(\vec{x}) = \gamma\}$, where γ represents the user specified iso-value. The surface which satisfies $\phi(\vec{x}) = \gamma$ is called the iso-surface (usually composed of a collection of triangles) [36].

Once the contour tracing algorithm generates triangular facets in those cubic cells crossed by the zero level set contours a mesh postprocessing (see Section 3.4) step has been proposed, which forms a closed iso-surface by connecting the common edges of the triangles in the entire volume. This extracted mesh can be directly used for the BE analysis without the need for any further discretisation. However, a mesh postprocessing step may be used, which makes the extracted mesh consistent with the BE analysis requirements.

3.4. Mesh postprocessing

The main steps followed in this process are discussed below.

(a) Mesh connectivity details

The standard MC algorithm generates at least one and as many as four triangles in each cubic cell of the level set grid crossed by the iso-surface. In order to analyse the re-constructed geometry with the BEM, these individual triangles need to be combined into a single closed iso-surface. Therefore, in this step, common vertices of the triangles in adjacent cells of the level set grid are replaced by a single vertex which results in a triangular mesh M with vertex set $V = 1, 2, \dots, n$, where n is the total number of vertices. Once we have the vertex connectivity details, the adjacent triangles to each triangle are identified. At this stage we ensure all triangles have a consistent and correct orientation as required for the BE analysis.

(d) Boundary conditions mapping

In the start of the optimisation process, the boundary conditions are assigned to the surface facets of the structural geometry. After the extraction of the modified structural geometry, the optimisation algorithm automatically maps the boundary conditions to those facets which overlap the bounding box for each set of the boundary conditions.

(e) Constraint locations fixing

In the present implementation, portion of the structural geometry belong to Γ_0 and Γ_1 are constrained against movement during the optimisation process. Once the boundary conditions are assigned to M , the set of vertices are split into two groups. Vertices are marked as fixed, V_f , or movable, V_m , depending on the boundary conditions prescribed. Only the set of vertices in V_m are allowed to be modified during the optimisation process.

3.5. Mesh improvements

As a result of the MC algorithm, the extracted surface models may contain many triangles with low quality (i.e. aspect ratio) [37]. In order to obtain accurate stress results using the BEM, it is expected that the extracted mesh should be of suitable quality. Therefore, some additional measures are always required, which can be seen as an enhancement of the MC algorithm, and it can be effectively incorporated into the computational codes. According to [38], the quality of an element can be assessed by the radius ratio, which is defined as the ratio of the radius of the incircle to the radius of the

circumcircle of the element. Mathematically it can be written as,

$$Q = \frac{16A^2}{L_1 \times L_2 \times L_3(L_1 + L_2 + L_3)} \quad (8)$$

where A is the area and L_1, L_2 and L_3 are the side lengths of the element. The value of Q varies between 0 and 1, where 1 indicates the highest quality (or in other words, an equilateral triangle) and 0 a fully collapsed element. As per the accuracy of the structural analysis results it is required that every element is of quality $Q > Q_{min}$, where Q_{min} is the minimum acceptable quality of the element. In addition to the element quality, high curvature values have also been observed at some portions of the mesh which may result in stress concentrations at those regions. In addition, the overall quality is assessed using the mean quality, \bar{Q} [39],

$$\bar{Q} = \frac{1}{N_E} \sum_{E=1}^{N_E} Q_E \quad (9)$$

where N_E represents the total number of elements and Q_E the quality of each element in a given mesh.

In order to improve the mesh quality, as well as to minimise the stress concentration effects, smoothing techniques may be required [37]. The most commonly used techniques are Laplacian and HC-Laplacian smoothing.

(a) *Laplacian smoothing*

A simple approach to mesh improvement which is often used is the Laplacian smoothing. In this approach, the new position of a vertex u_i is computed by averaging the location of the neighbouring vertices, i.e. $Adj(i)$ as shown in Figure 2 and given by,

$$u'_i = \begin{cases} \frac{1}{|Adj(i)|} \sum_{j \in Adj(i)} u_j & i \in V_m \\ u_i & i \in V_f \end{cases} \quad (10)$$

The new position of u'_i can be calculated by two methods [40]. In the first method, known as the simultaneous version, the new positions are calculated for all u_i , i.e. using the same set of positions. The second method updates the u_i immediately after the new position calculation. This method is known as the sequential version. In the second method the new position of u_i depends

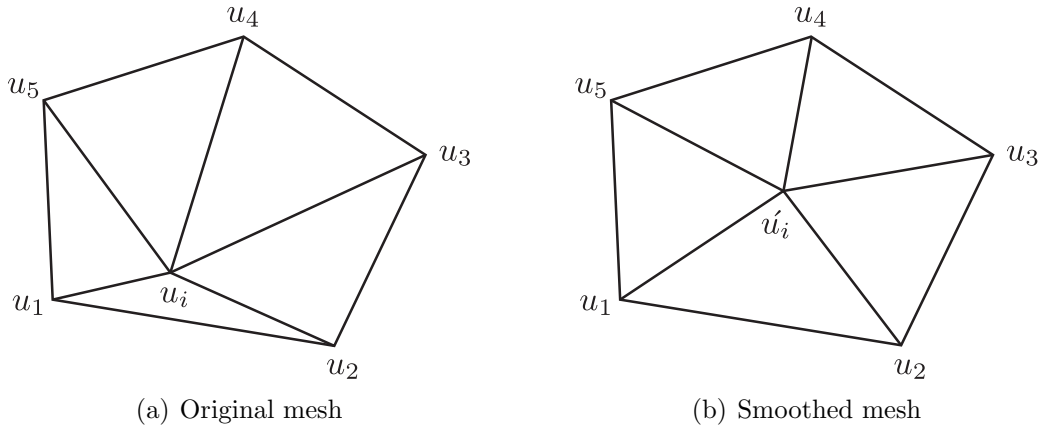


Figure 2: Laplacian smoothing

on both old and new positions. The results of the simultaneous version are better than the sequential one but this requires more storage space for holding the old positions.

In order to evaluate the performance of the Laplacian smoothing algorithm the extracted mesh of a short cantilever beam (see Section 4.1) at optimisation iteration 10 is considered. This initial mesh has fixed vertices at the constrained locations and movable everywhere else. Figure 3 shows contours of the mesh quality Q calculated through Equation (8) after 0, 5, 10, 15 and 20 iterations (smoothing steps), using the simultaneous version of the Laplacian algorithm. Low quality elements in the initial mesh depicted in Figure 3(a) can be clearly observed. In fact, this particular mesh contains some fully collapsed elements with $Q = 0$, which are improved after some iterations of Laplacian smoothing as shown in Figure 3(b)-(e). However, the results for 5, 10, 15 and 20 smoothing steps demonstrate considerable volumetric shrinkage and therefore, it is not recommended.

(b) HC-Laplacian smoothing

In order to reduce the shrinkage effect of Laplacian smoothing, Vollmer *et al.* [40] introduced the HC-Laplacian algorithm. Based on this modified approach, the vertices moved by the Laplacian smoothing are pushed back towards their previous positions u_i . The algorithm calculates the magnitude and direction of the backward movements from the original and previous vertex location using the weight ψ and the mean displacement vector in the neighborhood using parameter β (see for details [40]).

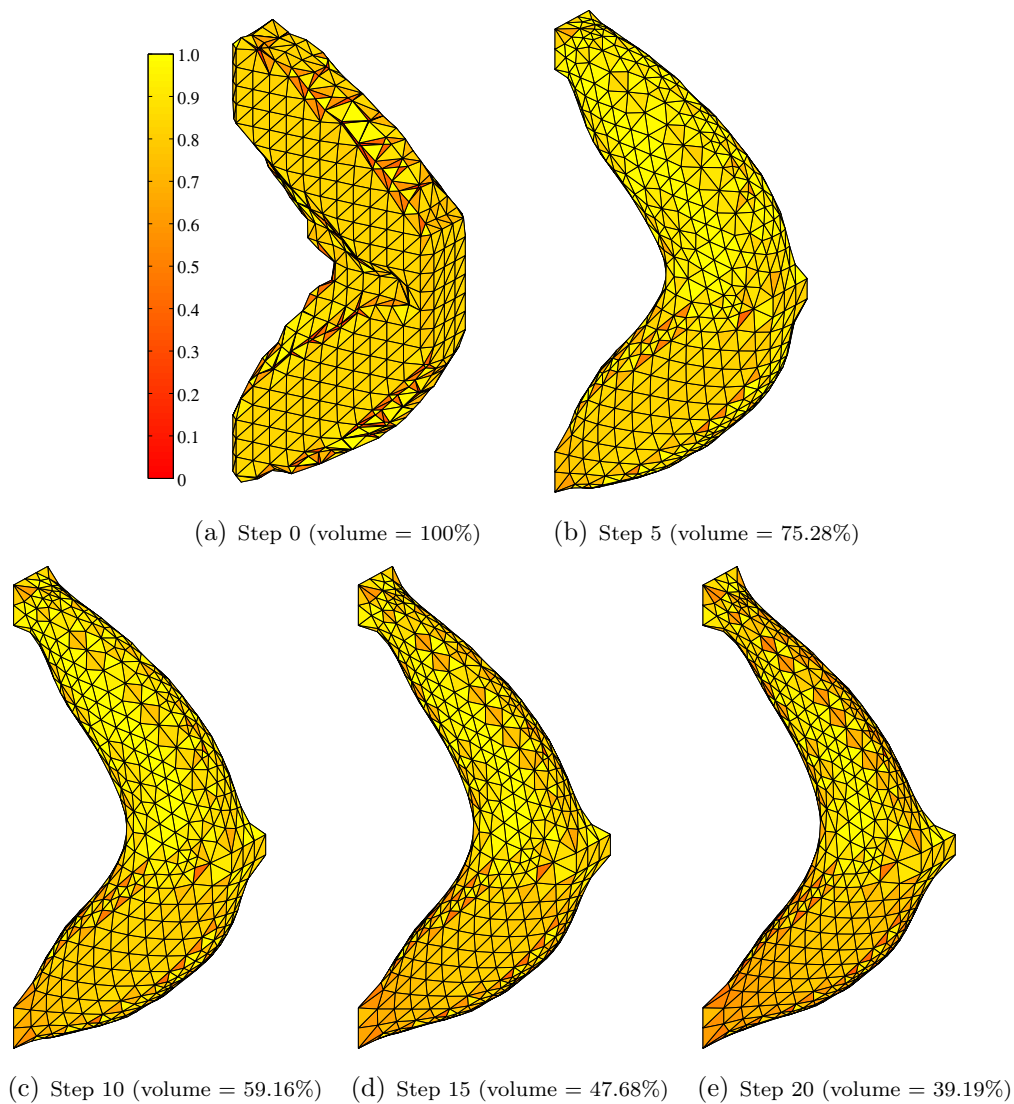


Figure 3: Mesh quality Q after 0, 5, 10, 15 and 20 Laplacian smoothing steps

Several iterations of the HC-Laplacian algorithm results in a sufficiently smoother mesh with little or no volume shrinkage. Following [40], the factors ψ and β used in the current implementation are set to 0.1 and 0.2, respectively. Figure 4 shows contours of the mesh quality Q calculated through Equation (8) after 0, 5, 10, 15 and 20 smoothing steps of the HC-Laplacian

algorithm. Additional mesh quality measurements with the HC-Laplacian algorithm with different smoothing steps are displayed in Table 1.

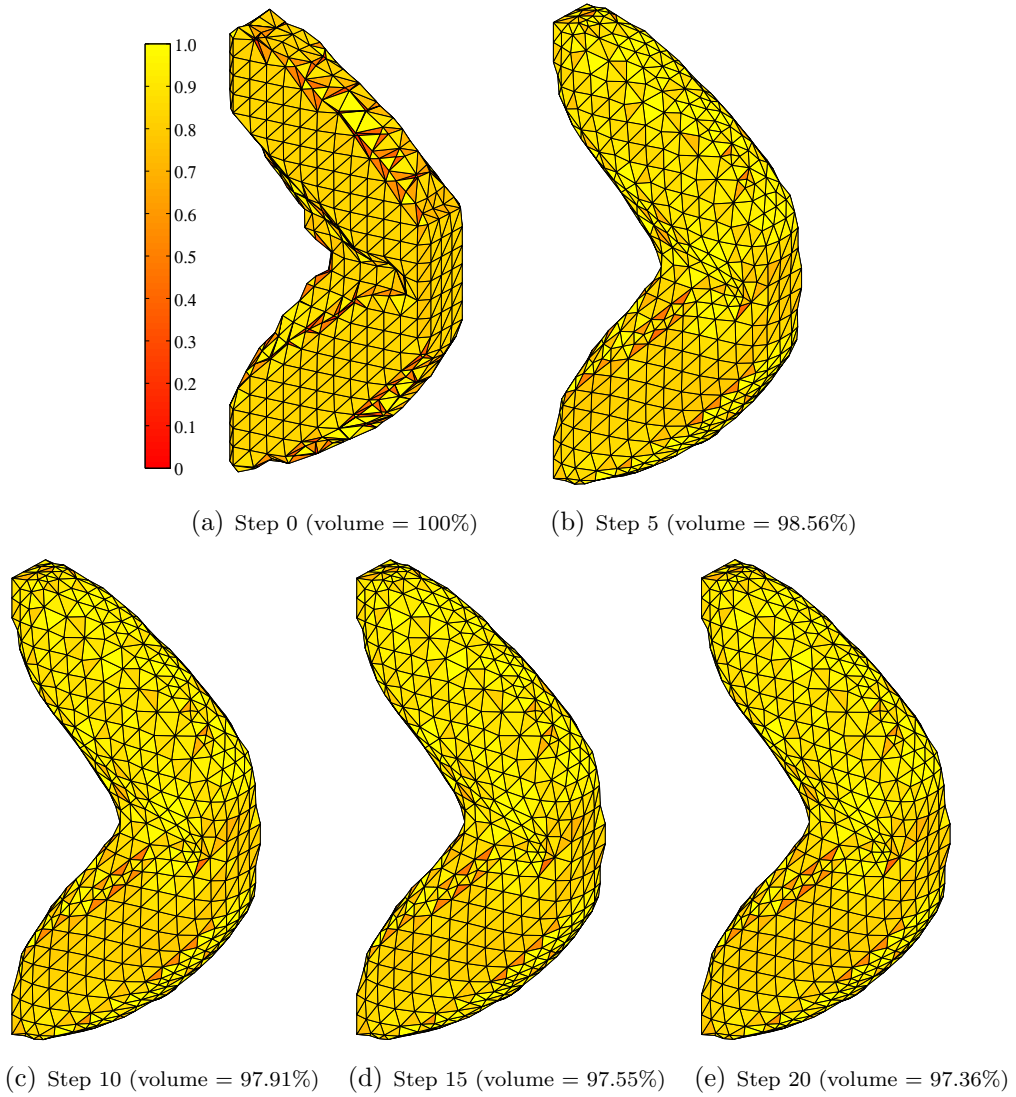


Figure 4: Mesh quality Q after 0, 5, 10, 15 and 20 HC-Laplacian smoothing steps

It is evident from Table 1 and Figure 4, that the HC-Laplacian algorithm significantly improves the individual element quality as well as the overall mesh quality. Bade *et al.* [37] also used the reduction in the mean of the

Steps	Total elements	Number of elements with Q_E				Q_{min}	\bar{Q}
		0 – 0.5	0.51-0.7	0.71 – 0.8	0.81 – 1.0		
0	1424	272	98	141	913	0.0	0.718
5	1424	16	66	114	1228	0.377	0.878
10	1424	8	73	89	1254	0.413	0.884
15	1424	8	71	81	1264	0.415	0.885
20	1424	7	73	80	1264	0.417	0.886

Table 1: Element quality data for HC-Laplacian smoothing

maximum curvature of the mesh as a smoothing criterion. Based on their results the mean of the maximum curvature of the surface decreases with an increase in the smoothing steps. On the other hand, the HC-Laplacian algorithm is not completely shrinkage free. Therefore, a suitable number of smoothing steps should be selected to obtain a good quality mesh with smoother geometry and low volume shrinkage. Based on the results presented in Table 1, Figure 4 and [37], we empirically found that a good choice would be to use 15 smoothing steps in each optimisation iteration.

In the present research work only the extracted structural model is used for the mesh improvement purpose, while the level set function is separately maintained by the Eulerian grid. Therefore, the low volume shrinkage associated with the HC-Laplacian smoothing has no effect on the implicit representation of the evolving structural model. Comparison of Figures 3(a) and 3(b-f) suggests that the proposed smoothing algorithm gradually modifies the low quality elements of the initially re-constructed structural model to enhance their quality from very low to an acceptable level. In addition, the Bi-directional nature of the proposed optimisation algorithm suggests that in case of any adverse effect associated with the volume shrinkage can automatically be handled in the current implementation.

3.6. The Boundary element analysis

The BEM is a standard technique for computational solution of partial differential equations. There are numerous textbooks describing the method (e.g. Becker [41]), but for completeness a brief description is included in this section.

We consider linear elasticity in the domain $\Omega \subset \mathbb{R}^3$, having boundary

$\partial\Omega = \Gamma$. We solve the equilibrium equations

$$\sigma_{ij,j}(\vec{x}) + b_i(\vec{x}) = 0, \quad \vec{x} \in \Omega \quad (11)$$

where $i, j = x, y, z$, the problem being subject to boundary conditions

$$u_i(\vec{x}) = \bar{u}, \quad \vec{x} \in \Gamma_u \quad (12)$$

$$t_i(\vec{x}) = \bar{t}, \quad \vec{x} \in \Gamma_t \quad (13)$$

In the above, u_i represents a displacement component, σ the Cauchy stress tensor and b the body force vector (per unit volume). We define $\Gamma = \Gamma_u \cup \Gamma_t$, but since it is commonplace in practice to prescribe different boundary condition types in different coordinate directions at the same point, this definition is purely symbolic. The traction component, t_i , is given by

$$t_i(\vec{x}) = \sigma_{ij}(\vec{x})n_j(\vec{x}), \quad \vec{x} \in \Gamma \quad (14)$$

where n is the unit outward pointing normal vector at \vec{x} . The terms \bar{u}, \bar{t} are prescribed known displacements and tractions respectively. The Einstein summation convention is assumed throughout. Taking for simplicity here the case $b = 0$, the differential equations (11) can be transformed into an equivalent integral equation form known as the Somigliana identity. We may write

$$c_{ij}(\vec{x})u_j(\vec{x}) + \int_{\Gamma} T_{ij}(\vec{x}, \vec{y})u_j(\vec{y})d\Gamma(\vec{y}) = \int_{\Gamma} U_{ij}(\vec{x}, \vec{y})t_j(\vec{y})d\Gamma(\vec{y}) \quad (15)$$

where T_{ij}, U_{ij} are respectively the traction and displacement kernels, or fundamental solutions. The free coefficients, c_{ij} , arise from the strong singularity in the integral containing the traction kernel; this integral is denoted \int to indicate its evaluation in the Cauchy Principal Value sense. The boundary may be discretised using elements, i.e.

$$\Gamma = \bigcup_{e=1}^{N_e} \Gamma_e, \quad \Gamma_i \cap \Gamma_j = \emptyset, i \neq j \quad (16)$$

and the geometry of each element parameterised in terms of a local intrinsic

coordinates $(\xi^e, \eta^e) \in [0, 1], e = 1, \dots, N_e$, allowing (15) to be rewritten

$$\begin{aligned} c_{ij}(\vec{x})u_j(\vec{x}) + \sum_{e=1}^{N_e} \sum_{l=1}^m \left[\int_{-1}^{+1} T_{ij}(\vec{x}, \vec{y}(\xi^e, \eta^e)) N_l(\xi^e, \eta^e) J^e(\xi^e, \eta^e) d\xi^e d\eta^e \right] u_j^{el} \\ = \sum_{e=1}^{N_e} \sum_{l=1}^m \left[\int_{-1}^{+1} U_{ij}(\vec{x}, \vec{y}(\xi^e, \eta^e)) N_l(\xi^e, \eta^e) J^e(\xi^e, \eta^e) d\xi^e d\eta^e \right] t_j^{el} \end{aligned} \quad (17)$$

where l is a local node number, on element e , that varies from 1 to $m = 3, 6, \dots$ for linear, quadratic elements etc., \vec{y} is the location on the element corresponding to the variable of integration ξ^e, η^e , N_l is the Lagrangian shape function for node l , J^e is the determinant of the Jacobian matrix of transformation and u_j^{el} and t_j^{el} are displacements and tractions, respectively, at local node l on element e . Taking point \vec{x} to be a node point, and evaluating the boundary integrals in (17) using a suitable scheme that copes with the singularities in the fundamental solutions, we arrive at

$$c_{ij}(\vec{x})u_j(\vec{x}) + \sum_{e=1}^{N_e} \sum_{l=1}^m h^{el} u_j^{el} = \sum_{e=1}^{N_e} \sum_{l=1}^m g^{el} t_j^{el} \quad (18)$$

where h^{el}, g^{el} are the evaluated integrals. Finally, placing point \vec{x} at each node in turn, equations of this form may be developed at each, and these may be assembled to form a linear system

$$[\mathbf{H}] \{\mathbf{u}\} = [\mathbf{G}] \{\mathbf{t}\} \quad (19)$$

where the matrices \mathbf{H} and \mathbf{G} contain the coefficients h^{el} and g^{el} respectively, and multiply vectors of nodal displacements and tractions. Application of the boundary conditions (12) and (13) reduces the problem to a square system that can be solved for unknown boundary displacements and tractions.

3.7. Boundary velocity computation

Once the BE analysis is carried out, the von Mises stress is calculated for each node point of the structural boundary as a post processing step. The von Mises stress at each node point is then converted into a scaled velocity through a stress velocity relationship presented in [27] and depicted in Figure 5; the intervals shown can be characterised in terms of σ_V (von Mises stress at a given node point), RR (removal ratio), σ_Y (Yield stress), and σ_{Vr} (reference von Mises stress), as follows:

- $\sigma_V \in [0, \sigma_{t1}] : \sigma_{t1} = 0.5 RR \sigma_{Vr}, F = -1$
- $\sigma_V \in [\sigma_{t1}, \sigma_{t2}] : \sigma_{t2} = 0.9 RR \sigma_{Vr}, F \in [-1, 0]$
- $\sigma_V \in [\sigma_{t2}, \sigma_{t3}] : \sigma_{t3} = 0.95 \min(\sigma_{Vr}, \sigma_Y), F = 0$
- $\sigma_V \in [\sigma_{t3}, \sigma_{t4}] : \sigma_{t4} = \min(\sigma_{Vr}, \sigma_Y), F \in [0, 1]$
- $\sigma_V \in [\sigma_{t4}, \infty) : F = 1$

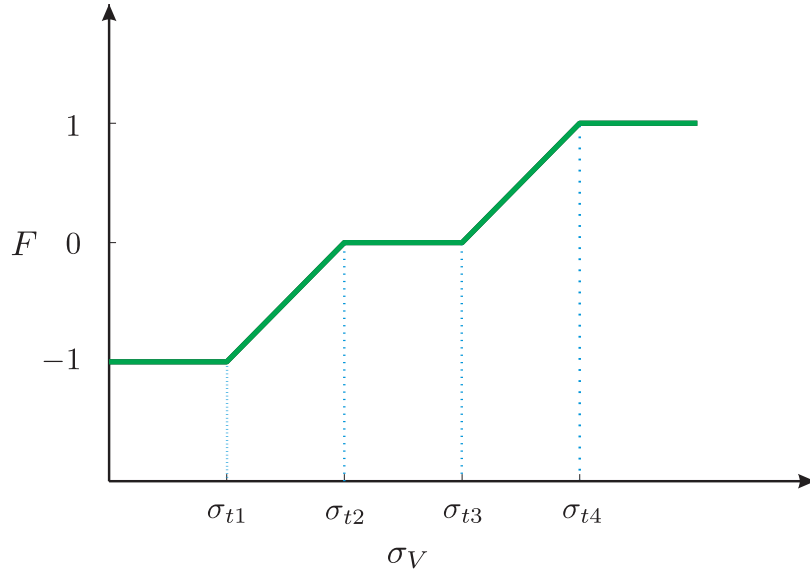


Figure 5: Conversion of σ_V to F

3.8. Velocity extension and update of the level set function

In the current implementation, the boundary velocity is extended to the level set grid using the method of Adalsteinsson and Sethian [42]. This method works on the simultaneous construction of the temporary signed distance function ϕ_t and extension velocity F_{ext} as follows,

$$\nabla \phi_t \cdot \nabla F_{ext} = 0 \quad (20)$$

The Fast Marching Method [29] is used for the construction of ϕ_t , which is based on the solution of the following Eikonal equation,

$$|\nabla \phi_t| = 1 \quad (21)$$

The level set function is re-initialised by the substitution of the temporary signed distance function ϕ_t for the current level set function. This provides a very fast and accurate way of re-initialisation of the level set function [29]. The re-initialisation can be carried out periodically as reported in [5]; however, the re-initialisation scheme adopted in the current implementation allows regularisation of the level set function at each optimisation step without any further computation. Moreover, computational efficiency is achieved by extending the boundary velocity to the grid points in the narrow band only [43].

After the velocity extension, the level set function is updated through the solution of Equation (1) with an upwind finite difference approximation [29]. The value of the time step size used in Equation (1) is based on the Courant-Friedrichs-Lewy (CFL) condition.

4. Examples

The validity and efficiency of the proposed optimisation method are tested against some benchmarking problems in the field of structural optimisation. The material properties used in these examples are: Poisson's ratio = 0.3, Young's modulus = 210 GPa, Yield stress = 280 MPa. For all examples, the optimisation process starts with evolutionary parameters, $RR = 0.01$ and $RR_i = 0.01$, unless otherwise stated.

During the numerical implementation for all examples, a fixed LS grid, composed of cubic cells with edge length $d = 2$ is specified over the entire design domain. In order to capture all possible boundary movements an additional row of cells is provided along each side of the LS grid. During the optimisation process, the surface mesh extracted from the LS grid is directly used as a discretised model of the evolving structural geometry. After carrying out the mesh post processing and improvement steps, the resulting quadratic triangular element based discretised structural model is analysed with the three-dimensional BEA software, i.e. 3D Concept Analyst [39]. The optimisation algorithm terminates when the given volume fraction has been achieved.

4.1. Example-1

In the first example, a short cantilever beam is considered with dimensions, $L = 24$, $W = 8$ and $H = 48$. The geometry of the structure, shown in Figure 6, is constrained at the top and bottom of the left face, and a load

$P = 1.2$ kN is applied at the middle of the right face. The level set design domain is discretised into $12 \times 4 \times 24$ cubic cells. The target volume fraction used in this example is $\alpha = 0.30$.

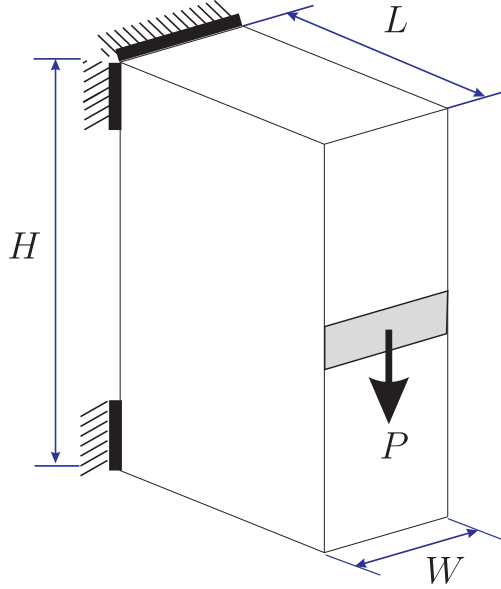


Figure 6: Design domain, loading and boundary conditions for Example-1

Figure 7 shows the evolution of the structural geometry of the short cantilever beam with $\sigma_{Vr} = \sigma_{Vmax} = 178$ MPa, where σ_{Vmax} is the maximum von Mises stress in the initial design. It can be seen that the incremental removal of the inefficient material from the low stressed regions of the structure gives rise to significant topological changes, i.e. automatic hole nucleation as shown in Figure 7(c). The final design displayed in Figure 7(d) is similar to that presented in [32, 44]. This suggests that optimal designs can also be obtained with the present method, which is capable of handling shape and topology simultaneously through boundary only perturbation.

Figure 8 shows the von Mises stress distribution for the initial and optimal designs, respectively. The optimisation process starts from an initial design domain with 1724 triangular elements as shown in Figure 8(a). Inefficient material is progressively removed from the low stressed regions of the structure and the optimisation process terminates at the target volume fraction with 1200 triangular elements in the final design as depicted in Figure

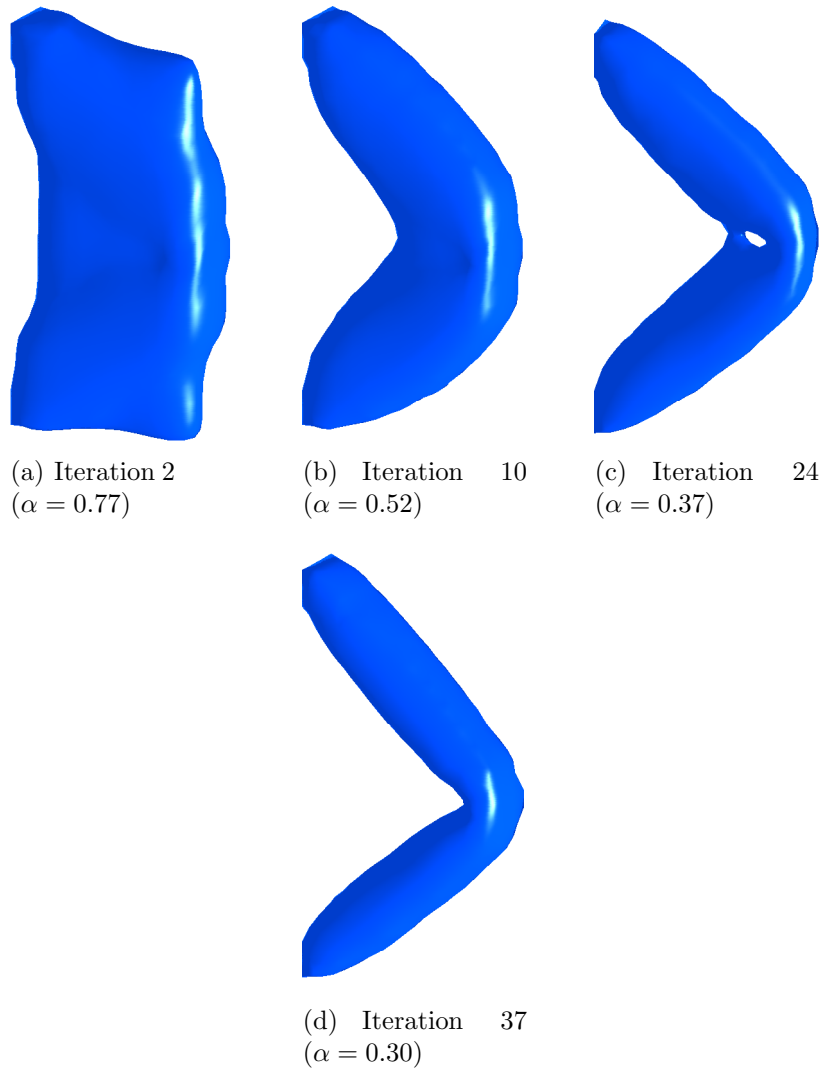


Figure 7: Evolution of structural geometry for Example-1, case 1

8(b). Comparison of the stress contours for the initial and optimal designs suggests that the stress contours are more uniform in the latter.

It should be noted that throughout the optimisation process the computation of the boundary stresses is sufficient to carry out changes in both shape and topology. This considerably reduces the computational burden

associated with the calculation of stresses within the design domain at each optimisation iteration and potential problems related to domain discretisation. This is a clear advantage of the proposed optimisation method over the available FE based optimisation approaches. Further, in the current implementation, the implicitly represented geometry is naturally linked with the structural model and thus provides a unified approach which completely automates the whole optimisation process without the need of an additional mesh generation technique.

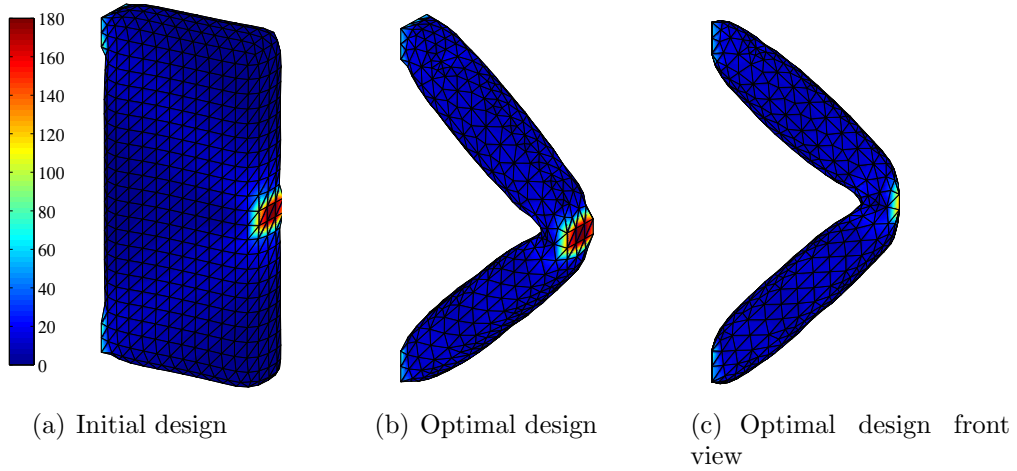


Figure 8: von Mises stress contours of initial and final optimal geometry for Example-1, case 1

During the optimisation process the evolution of the specific strain energy is recorded at each optimisation iteration and is depicted in Figure 9. It can be observed that f_U decreases quickly during the initial iterations, which is mainly related to the rapid removal of the inefficient material from the design domain. In the following iterations, a decrease in the material removal rate causes a slow decrease in f_U up to the end of the optimisation process.

In order to investigate the effect of the stress criterion values on the final optimal solution, this topology optimisation problem is further solved with $\sigma_{Vr} = 100$ MPa and 50 MPa, respectively. Figure 10 displays the von Mises stress contours of optimal designs for all three cases in this example. A comparison of these cases suggests that the proposed optimisation method provides similar optimal configurations both from geometric as well as stress

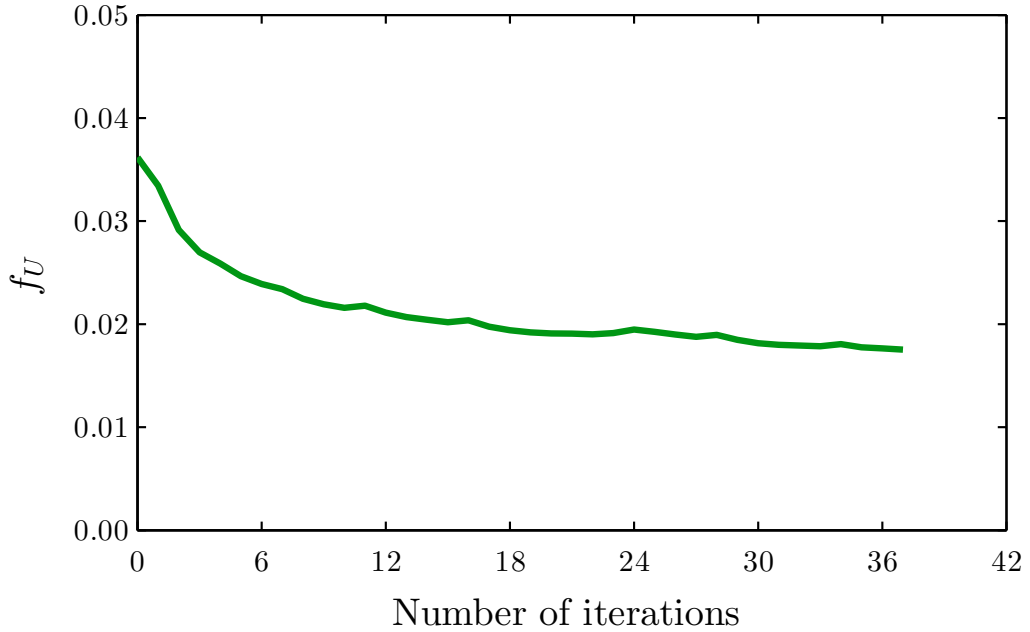


Figure 9: Evolution of f_U for Example-1, case 1.

distribution points of view. However, it can be seen from Table 2 and Figure 11 that a reduction in σ_{V_r} decreases the material removal rate, and consequently; more optimisation iterations are used to achieve the same target volume fraction. However, in all three cases, the optimisation process terminates around the same values of f_U with $\sigma_{V_r} \leq \sigma_{V_{max}}$. On the other hand, the use of $\sigma_{V_r} > \sigma_{V_{max}}$ may increase the material removal rate, and would provide final designs having higher f_U for the same target volume fraction. This comparison suggests that the use of $\sigma_{V_r} = \sigma_{V_{max}}$ as a stress criterion for the optimisation process provides optimal designs with fast convergence.

Case	σ_{V_r} (MPa)	Total iterations	Final f_U (Nmm ⁴)
1	178	37	0.0175
2	100	54	0.0188
3	50	107	0.0175

Table 2: Comparison of f_U for Example-1

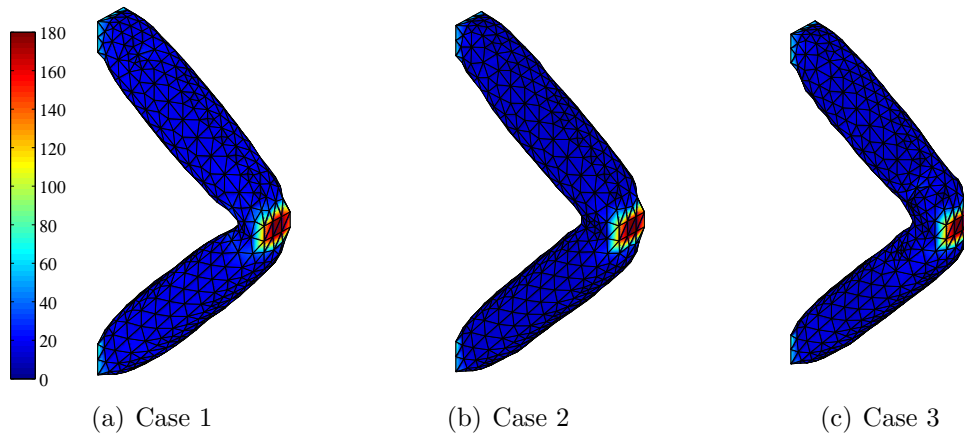


Figure 10: von Mises stress contours of optimal designs for Example-1 with $\alpha = 0.30$ and different σ_{Vr}

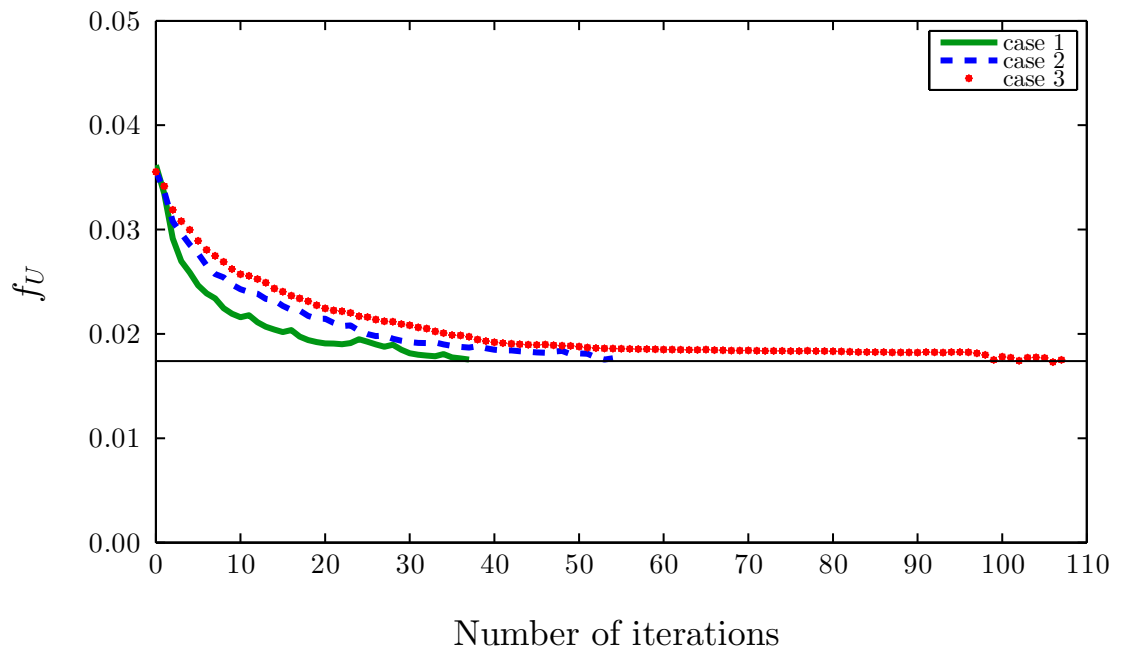


Figure 11: Evolution of f_U for Example-1

4.2. Example-2

The second example considered in this study is a short cantilever beam with dimensions $L = 40$, $W = 8$ and $H = 40$. The structural geometry shown in Figure 12 is constrained at the top and bottom of the left face, and a load $P = 2.4$ kN is applied at the right hand end of the bottom face. The level set design domain is discretised into $20 \times 4 \times 20$ cubic cells. The optimisation problem is solved for $\alpha = 0.35$.

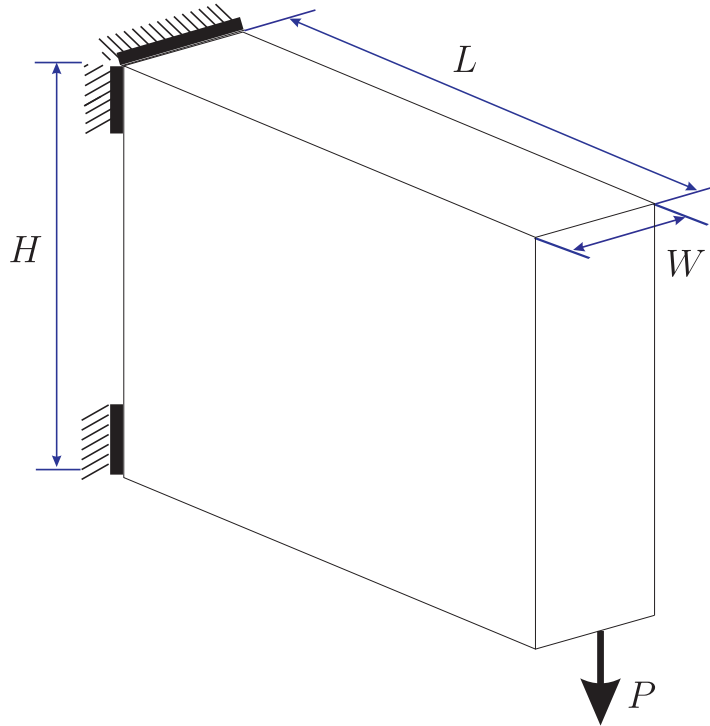


Figure 12: Design domain, loading and boundary conditions for Example-2

To further validate the proposed optimisation method with different loading conditions, the optimisation problem in this example is solved with two different stress criterion, i.e. $\sigma_{Vr} = \sigma_{Vmax}$ and $\sigma_{Vr} < \sigma_{Vmax}$. Figure 13 shows the evolution of the structural geometry with $\sigma_{Vr} = \sigma_{Vmax} = 260$ MPa. It can be seen that in the initial iterations most of the inefficient material removal is handled through shape optimisation only. Nucleation of new holes can be observed in the subsequent iterations as depicted in Figure

13(b-e), which demonstrates the automatic hole nucleation capability of the proposed optimisation method. Throughout the optimisation process, holes appear, evolve and merge together, leading this way the structural geometry towards the target volume fraction.

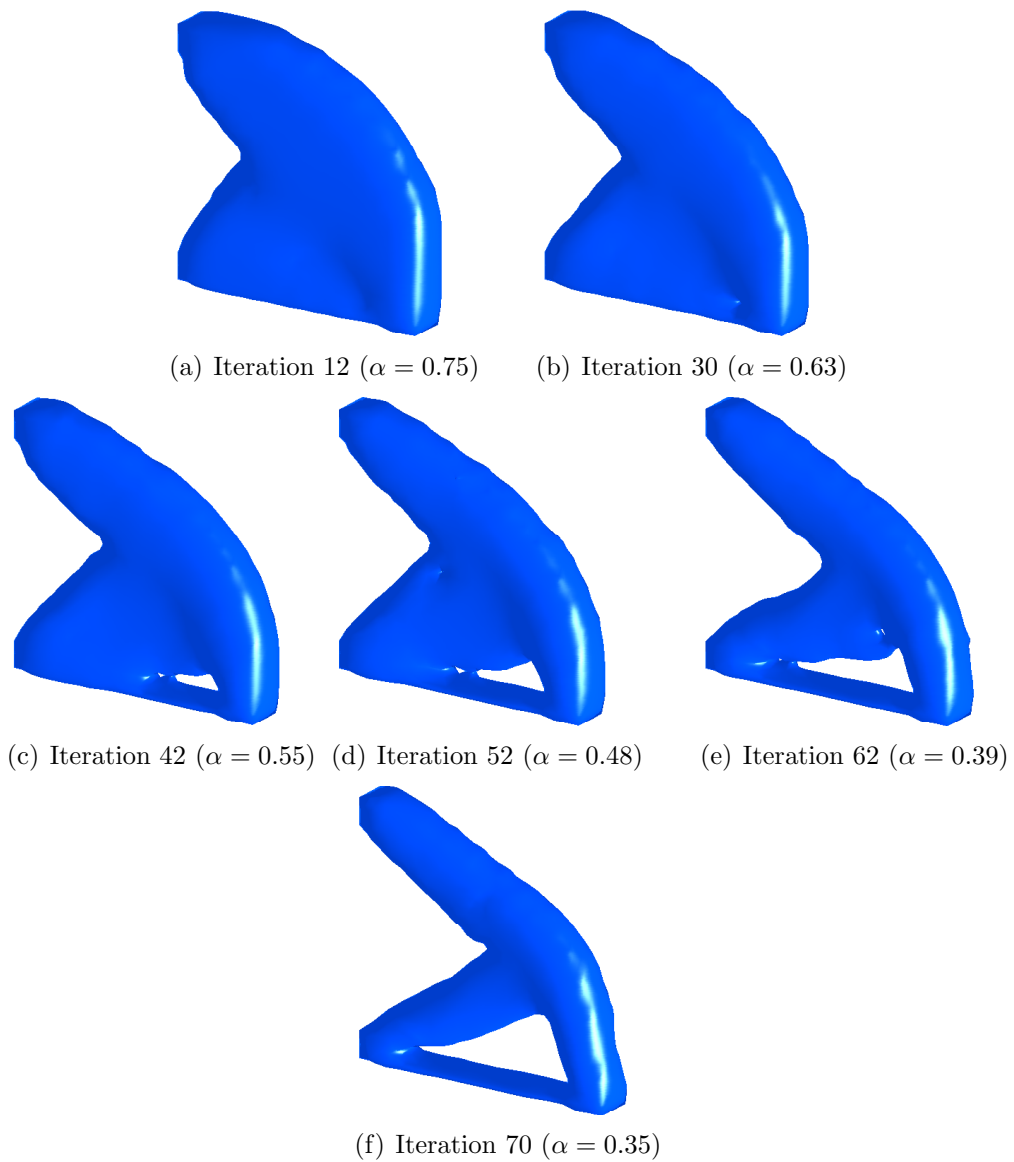
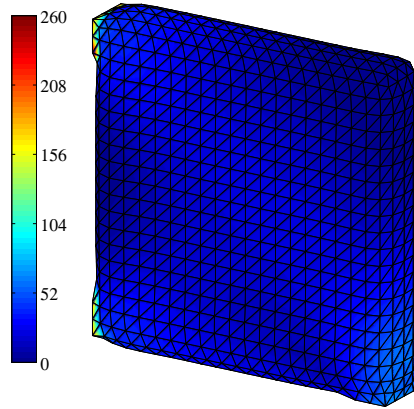


Figure 13: Evolution of structural geometry for Example-2, case 1

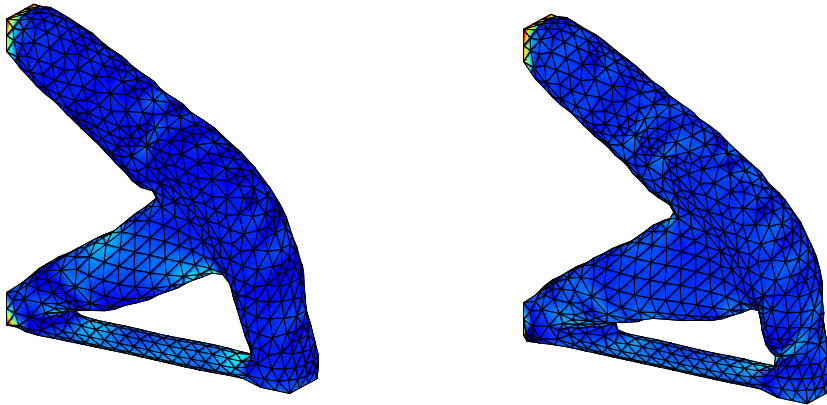
The optimal structure depicted in Figure 13(f) is similar to that reported for a two-dimensional case in [48] and a corresponding three-dimensional case in [44, 49]. Hence, this close agreement between the optimal solution obtained by the proposed method and the classical optimisation approaches, e.g. [48] and the added advantages of dimensionality reduction and simplification of re-meshing at each optimisation step suggest that the proposed method can be very beneficial for the solution of three-dimensional topology optimisation problems.

The optimisation problem in this example is further solved with $\sigma_{Vr} = 100$ MPa, and the optimal design obtained after 114 iterations is depicted in Figure 14(c). For comparison purpose, the von Mises stress contour plots of the initial and optimal designs (for both cases) are displayed in Figure 14. It can be seen that in both cases, the proposed optimisation method results in very similar optimal geometries and with analogous stress distribution. However, as observed in Example-1 too, with the use of $\sigma_{Vr} < \sigma_{Vmax}$, the same target volume fraction has been achieved in more iterations as compared to the first case of this example.

Figure 15 shows a comparison of the evolution of f_U in both cases of this example. It can be seen that a relatively high material removal rate rapidly decreases f_U in the initial iterations. Once most of the inefficient material is removed, a slow decrease can be observed in the following iterations. Finally, the optimisation processes terminates with a difference of approximately 3% in the final values of f_U .



(a) Initial design ($\alpha = 0.35$)



(b) $\sigma_{Vr} = 260$ MPa ($\alpha = 0.35$, iterations 70) (c) $\sigma_{Vr} = 100$ MPa ($\alpha = 0.35$, iterations 114)

Figure 14: von Mises stress contours of optimal designs for Example-2

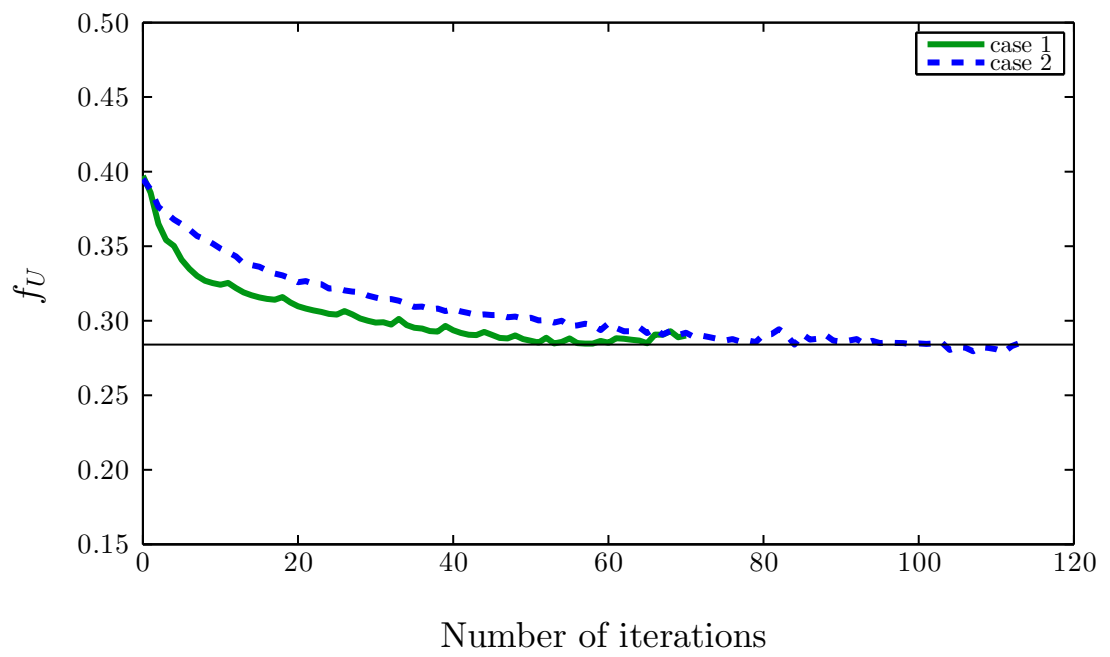


Figure 15: Evolution of f_U for Example-2

4.3. Example-3

The proposed optimisation method is further tested against another benchmark problem of a short cantilever beam with dimensions $L = 40$, $W = 8$ and $H = 24$. The structural geometry and loading and boundary conditions are depicted in Figure 16. The optimisation problem is solved with $P = 1.2$ kN and $\alpha = 0.30$. The level set design domain is discretised into $20 \times 4 \times 12$.

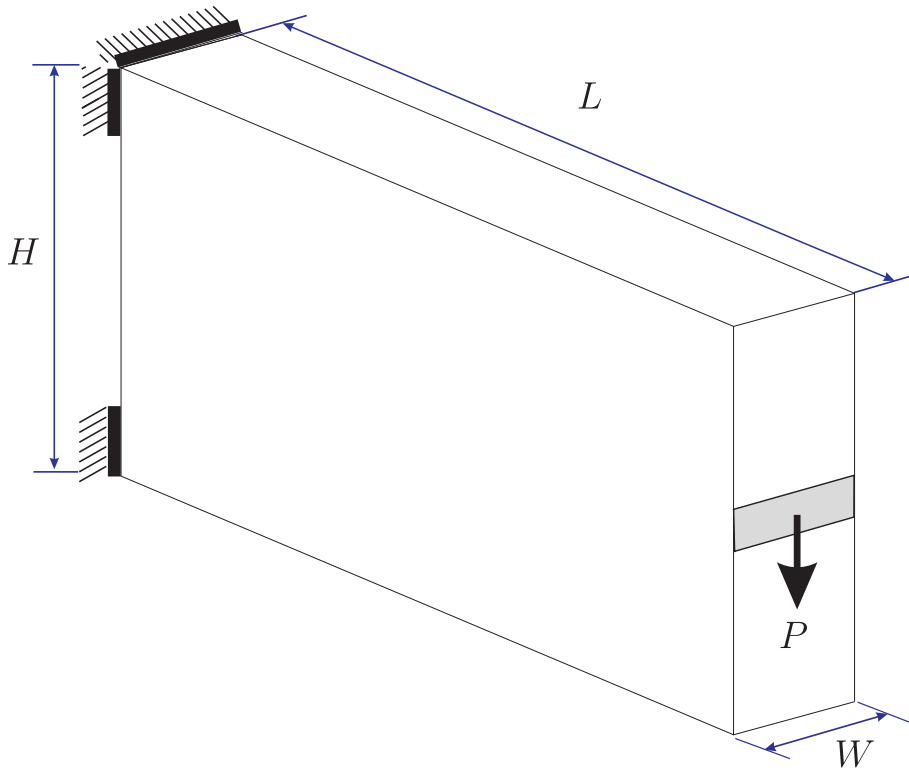


Figure 16: Design domain, loading and boundary conditions for Example-3

Figure 17 shows evolution of the structural geometry at different stages of the optimisation process. It can be seen that the initial geometry evolves into an optimal design through boundary movements, which also allows hole nucleation and its immediate merging with the existing holes. The multiple cavities based final optimal design obtained in this example demonstrates the effectiveness of the proposed method in handling complex topological

changes during the optimisation process. The final design obtained for this type of problem is similar to the optimal configuration using the FEM based BESO approach [50] and the level set based optimisation method presented in [19, 51]. The proposed optimisation method provides fast convergence of the optimal solutions. This is evident from the optimisation history presented in Figure 17 where the optimal solution converged in 32 iterations, which are less than the 80 iterations used in [51] and 226 in [50]. Moreover, the use of a boundary discretisation approach provides computational efficiency as well as relieving the complexity associated with the domain discretisation of a continuously evolving structural model in a three-dimensional topology optimisation. However, at the same time, the use of quadratic elements in the current implementation gives a much higher fidelity of the solution than the four noded square elements used in [50] and tetrahedral elements in [51].

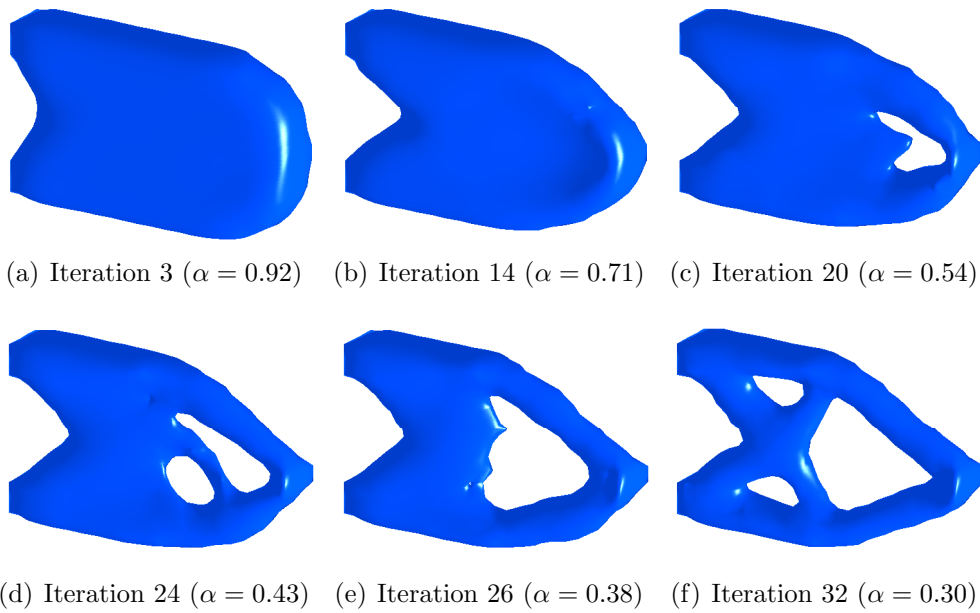
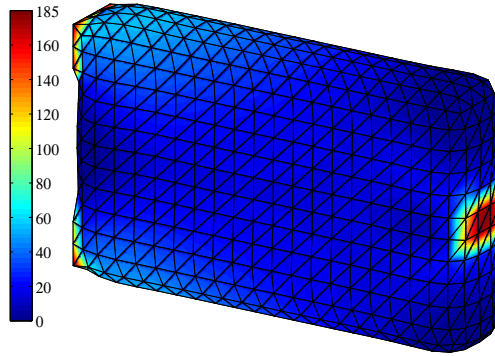


Figure 17: Evolution of structural geometry for Example-3

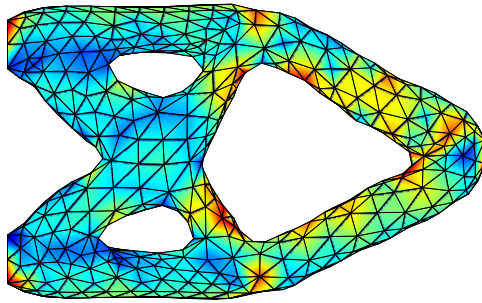
Figure 18 shows the von Mises stress contour plots for the initial and optimal designs. There are 1468 triangular elements in the initial and 1384 in the final design, respectively. A uniform stress distribution can be observed in the

optimal design, which suggests that the optimisation method redistributes the material within the design domain through the progressive removal of inefficient material from the low stressed regions and addition of efficient material at high stressed regions and works like a descent method. This can be further verified from the cross-sectional variation of the structural members in the optimal configuration. Comparison of the stress contours suggests that an almost fully stressed optimal design is reached in this example. This further reflects that the proposed optimisation method fulfills the required optimality conditions and indicates that a shape optimisation is achieved. Further, the cross-sectional variation of the optimum structure members depicted in Figure 18(d) is analogous to those presented in [19, 50]; hence, this validates the proposed approach for the solution of three-dimensional topology optimisation problems.

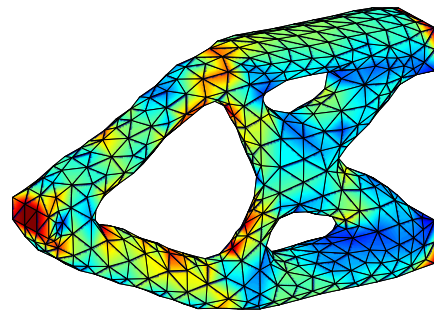
Figure 19 shows the evolution of f_U during the optimisation process. Apart from the interval between iterations 18 to 30, a smooth progression can be observed during the evolution of f_U . The interval between iterations 18 to 24 is mainly related to the removal of material through hole nucleation as shown in 17(c) and (d). A high peak can be observed at iteration 25, caused by a significant change in the topology resulting from the elimination of a bar in one iteration (related to hole merging), as can be seen from Figures 17(d) and (e). The occurrence of high peak in the solution of a similar problem in two-dimensions has also been observed in a BESO based approach presented in [45], and is therefore not unique to our approach. The effect of this high peak dies out quickly in the proceeding iterations and f_U slowly decreases until the target volume fraction is reached.



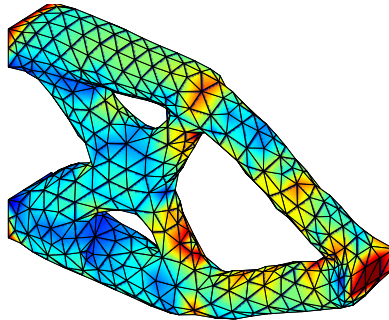
(a) Initial design



(b) Optimal design view 1



(c) Optimal design view 2



(d) Optimal design view 3

Figure 18: von Mises stress contours of initial and optimal geometry for Example-3

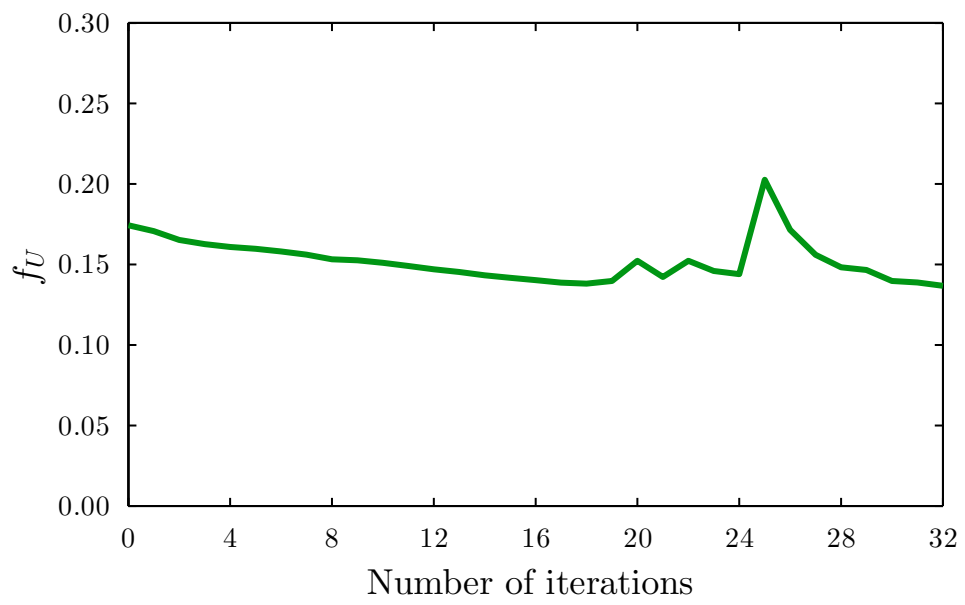


Figure 19: Evolution of f_U for Example-3

4.4. Example-4

The final example solved in this study is a cube with dimensions, $L = 26$, $W = 26$ and $H = 26$, as shown in Figure 20. Based on the boundary conditions, three different cases are considered for this example. In the first case, a load $P = 1.6$ kN is applied at the centre of the top face, and the bottom face is constrained in all directions at the four corners. In the second case, three of the fixed constraints are replaced by roller supports. The third case is similar to the first one; however, the load is applied at the whole area of the top face. In all cases, the level set design domain is discretised into $13 \times 13 \times 13$ cubic cells.

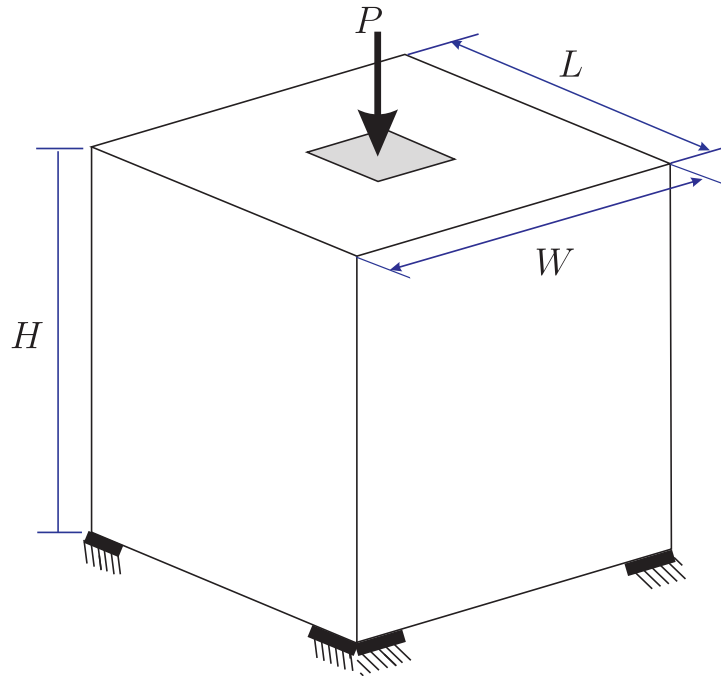


Figure 20: Design domain, loading and boundary conditions for Example-4

In case 1, the optimisation problem is solved with $\sigma_{Vr} = \sigma_{Vmax} = 55$ MPa and $\alpha = 0.30V_0$. The evolution of the structural geometry during the optimisation iterations is depicted in Figure 21. The optimal solution depicted in Figure 21(d) is similar to those reported in [44, 46]. The corresponding von Mises stress contour plots for the initial and optimal designs are displayed in Figure 22.

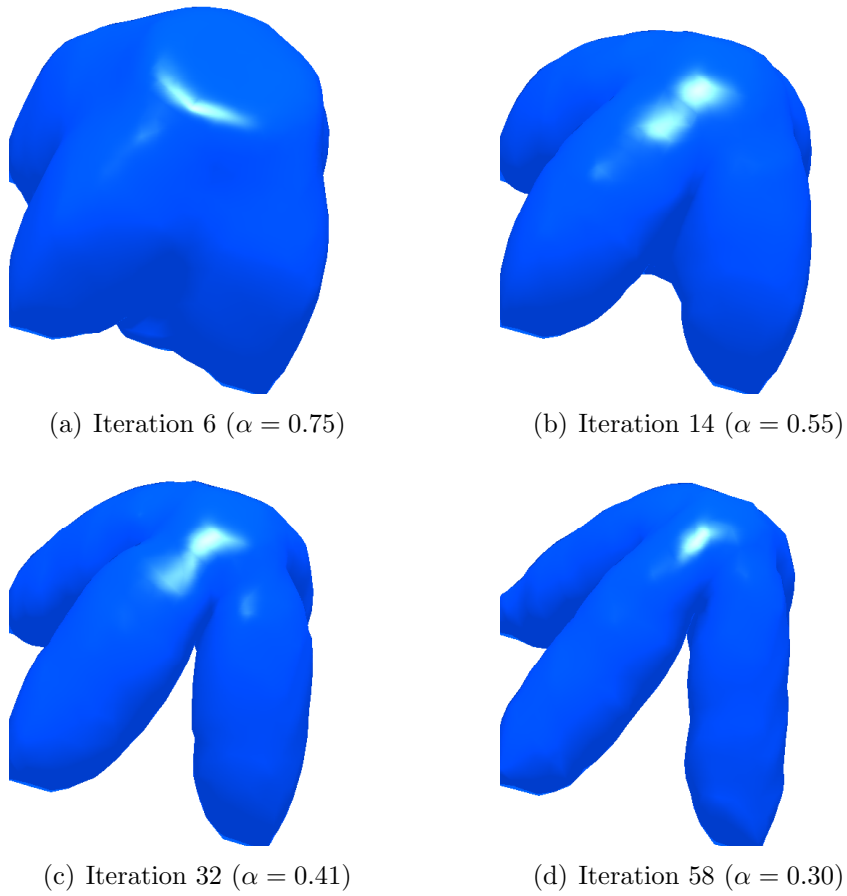


Figure 21: Evolution of structural geometry for Example-4, case 1

Figure 23 shows the evolution of the specific strain energy during the optimisation process. It can be seen that in the initial iterations the specific strain energy decreases rapidly due to fast material removal, settling down near the end of the optimisation process.

In case 2 of this example, three fixed constraints are replaced with roller supports whereas the initial design and loading are kept the same as in case 1. The optimisation problem is solved with $\sigma_{Vr} = \sigma_{Vmax} = 53$ MPa and $\alpha = 0.30V_0$. The evolution of the structural geometry at different stages of the optimisation process is displayed in Figure 24. Compared to case 1, as expected, the use of roller supports resulted in interconnecting bars between

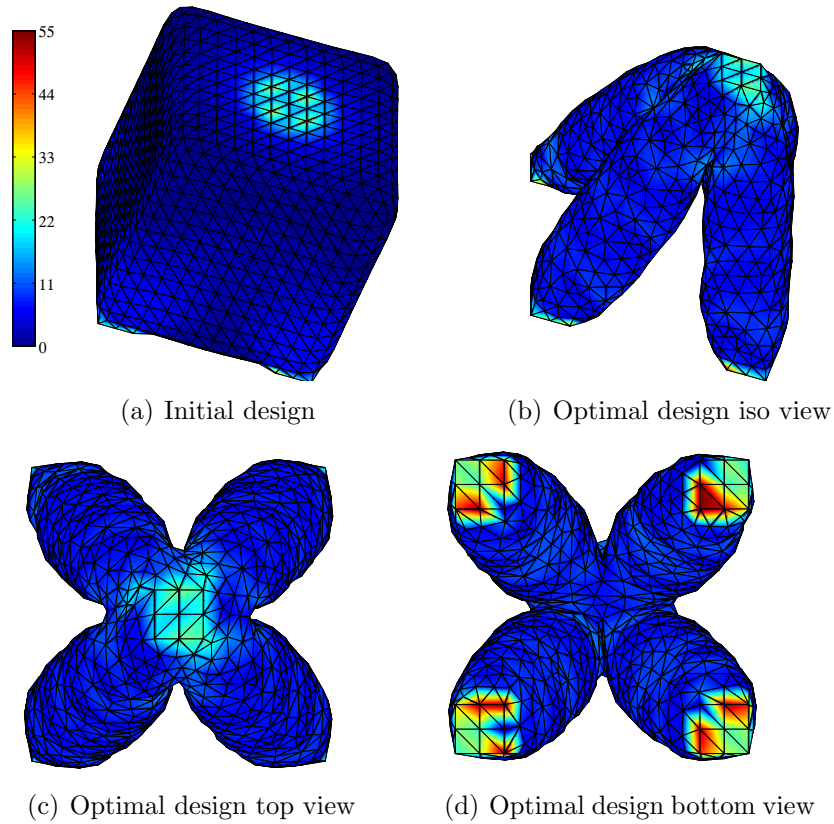


Figure 22: von Mises stress contours of initial and optimal geometry for Example-4, case 1

the four supporting members of the structure. The final design shown in Figure 24(d) is similar to those presented in [44, 47, 46].

The optimisation problem for a similar initial design used in the second case of this example has also been solved in [44, 47]. In those studies, design modifications were based on the topological derivative approach; the linear elasticity problem was solved with the FEM and mesh refining algorithms. The topological derivative approach used in [47] is further studied within a BEM framework by Bertsch *et al.* [46]. In their implementation, the structural boundary was discretised using constant quadrilateral elements, and a regular array of internal points was used inside the design domain. The modified geometry was re-meshed at each optimisation step. It can be

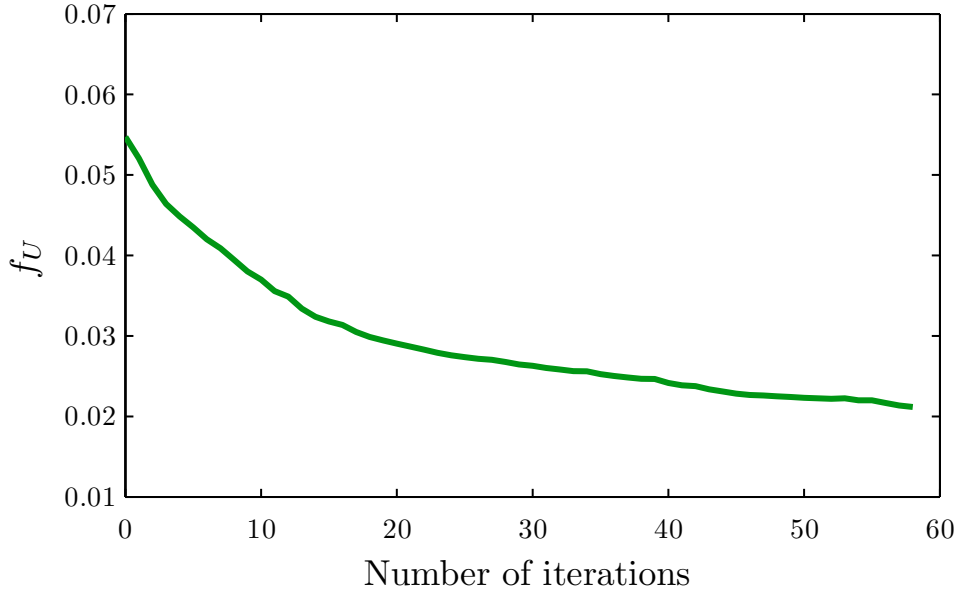


Figure 23: Evolution of f_U for Example-4, case 1

seen that in [44, 47, 46] computation of the structural response at the design boundary as well as within the design domain is an essential part of the optimisation process. However, in the present research work improvements in both shape and topology are accomplished with the evaluation of structural response along the design boundary only. Moreover, the quadratic elements give a much higher fidelity of the solution than the constant element models of [46]. The obtained optimised structure as depicted in Figure 24(d) is very similar to the results presented in [44, 47, 46], we consider that this agreement gives supporting evidence for the usefulness of the proposed optimisation method. In the current implementation a volume fraction of 0.30 is achieved in only 34 iterations. However, as reported in [46], volume fractions of 0.80 and 0.04 have been achieved in 200 and 960 optimisation steps, respectively, which suggests that the proposed optimisation algorithm is computationally more efficient and robust. Additionally, the MC algorithm places the mesh vertices on the edges between the grid nodes, the mesh resolution is not constrained by the resolution of the grid. Thus, the proposed method avoids

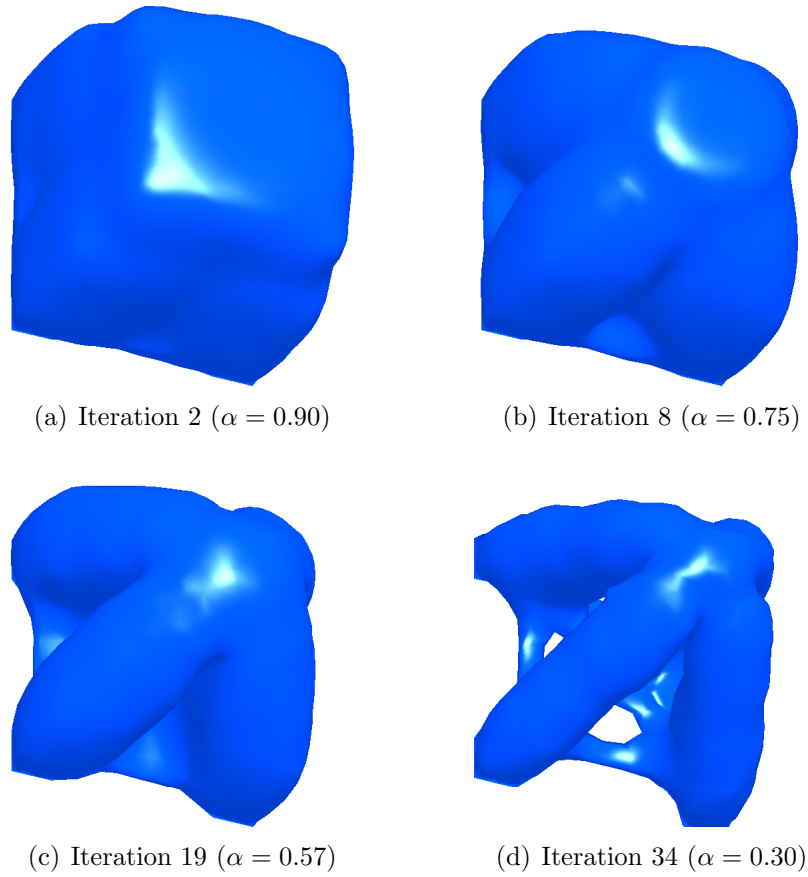


Figure 24: Evolution of structural geometry for Example-4, case 2

the blocky artifacts that can be noticed in [46], and the final optimal design can be directly used in other design processes. The bi-directional nature of the proposed optimisation algorithm, which adds and removes material simultaneously makes this algorithm practically more applicable than [46], in which design modifications are based on material removal only.

In the final case of this example, the boundary conditions are those as used in case 1, however, the load is now applied at the whole face. Figure 26 shows several intermediate results obtained during the optimisation process. While in the previous two cases the optimum designs have inclined supporting members, in case 3, with different loading conditions, the optimisation method resulted in a final design with straight supporting members as shown

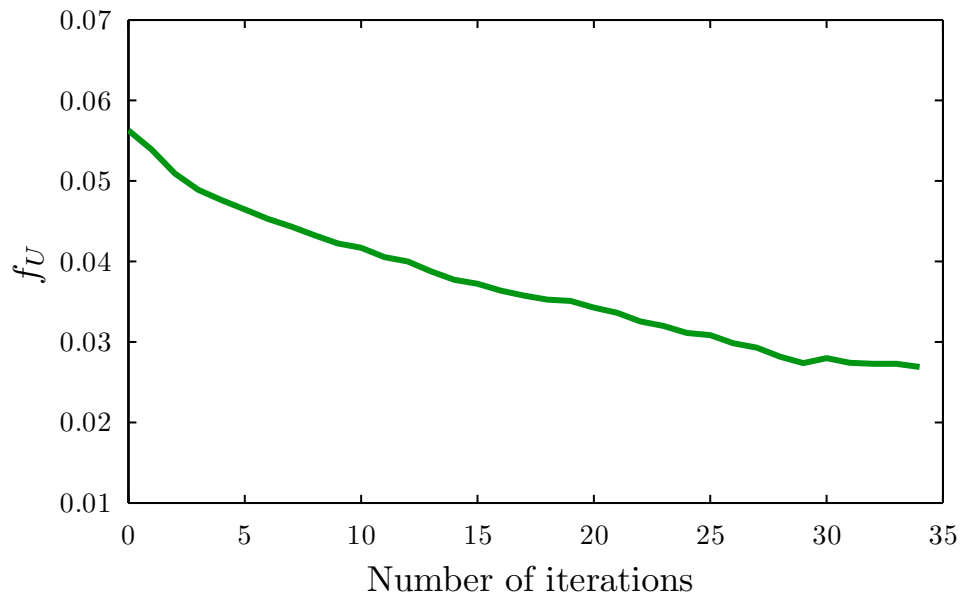


Figure 25: Evolution of f_U for Example-4, case 2

in Figure 26(d). This final case demonstrates that the proposed optimisation method can be efficiently used for solving a range of optimisation problems.



(a) Iteration 3 ($\alpha = 0.90$)



(b) Iteration 20 ($\alpha = 0.80$)



(c) Iteration 35 ($\alpha = 0.70$)

5. Conclusions

A three-dimensional topology optimisation method is presented in this paper. During the optimisation process, the structural geometry evolves into an optimal design through the progressive removal of inefficient material from the low stressed regions and addition of efficient material to the high stressed regions of the structure. This evolutionary approach is integrated with the boundary element and level set methods. The boundary based discretisation approach, i.e. BEM is used to predict the structural response along the continuously evolving structural boundary at each optimisation iteration. The optimisation method identifies potential regions along the structural boundary to be modified and is evolved through the solution of the HJ type level set equation.

As demonstrated through the examples presented, in three-dimensional LSM based optimisation, holes appear automatically through the intersection of two surfaces moving towards each other. Therefore, in three-dimensional optimisation, the use of LSM eliminates the need for an additional hole insertion mechanism as both shape and topology optimisation take place simultaneously. During the optimisation iterations, the MC algorithm extracts the modified geometry (i.e. the zero level set contours) in the form of a triangular mesh. However, there may exist some low quality elements in the extracted mesh, which can reduce the accuracy of the BE solutions, a mesh postprocessing and improvement step is used to enhance the quality of the individual elements as well as the overall mesh. The integration of the BEM and LSM through an MC algorithm eliminates the need for a conventional BEM meshing tool since the meshing is performed directly as part of the described optimisation algorithm; this provides a natural link between the implicitly represented geometry and structural model.

The proposed method is validated with four different benchmark examples. Each example is further solved with different stress criteria, and similar optimal designs are obtained for each case. The optimal designs obtained for each example closely resemble the optima published within the field of structural optimisation.

In this initial implementation the surface mesh size is dependent on the level set grid resolution. Based on the numerous numerical tests conducted a suitable level set grid size is used in all examples (having different geometric configurations, loading and boundary conditions), and results obtained are similar to those available in the literature. In the next phase of this research

study, the performance of the proposed approach can be further improved by the introduction of adaptivity in both the BE analysis and local level set grid size refinement.

Acknowledgements

The first author acknowledges with thanks the financial support through the Durham Doctoral Studentship scheme of the Durham University.

References

- [1] S. Osher, J. A. Sethian, Front propagating with curvature-dependent speed: algorithms based on Hamilton-Jacobi formulations, *Journal of Computational Physics* 79 (1) (1988) 12–49.
- [2] J. A. Sethian, A. Wiegmann, Structural boundary design via level set and immersed interface methods, *Journal of Computational Physics* 163 (2) (2000) 489–528.
- [3] S. J. Osher, F. Santosa, Level set methods for optimization problems involving geometry and constraints: I. frequencies of a two-density inhomogeneous drum, *Journal of Computational Physics* 171 (1) (2001) 272–288.
- [4] M. Y. Wang, X. Wang, D. Guo, A level set method for structural topology optimization, *Computer Methods in Applied Mechanics and Engineering* 192 (1-2) (2003) 227–246.
- [5] G. Allaire, F. Jouve, A. M. Toader, Structural optimization using sensitivity analysis and a level-set method, *Journal of Computational Physics* 194 (1) (2004) 363–393.
- [6] N. P. Dijk, K. Maute, M. Langelaar, F. Keulen, Level-set methods for structural topology optimization: a review, *Structural and Multidisciplinary Optimization* 48 (3) (2013) 437–472.
- [7] O. Sigmund, J. Petersson, Numerical instabilities in topology optimization: A survey on procedures dealing with checkerboards, mesh-dependencies and local minima, *Structural optimization* 16 (1) (1998) 68–75.

- [8] G. W. Jang, Y. Y. Kim, Sensitivity analysis for fixed-grid shape optimization by using oblique boundary curve approximation, *International Journal of Solids and Structures* 42 (11–12) (2005) 3591–3609.
- [9] S. Yamasaki, T. Yamada, T. Matsumoto, An immersed boundary element method for level-set based topology optimization, *International Journal for Numerical Methods in Engineering* 93 (9) (2013) 960–988.
- [10] S. Y. Wang, K. M. Lim, B. C. Khoo, M. Y. Wang, An extended level set method for shape and topology optimization, *Journal of Computational Physics* 221 (1) (2007) 395–421.
- [11] J. Luo, Z. Luo, L. Chen, L. Tong, M. Y. Wang, A semi-implicit level set method for structural shape and topology optimization, *Journal of Computational Physics* 227 (11) (2008) 5561–5581.
- [12] S. Wang, M. Y. Wang, A moving superimposed finite element method for structural topology optimization, *International Journal for Numerical Methods in Engineering* 65 (11) (2006) 1892–1922.
- [13] T. Fries, T. Belytschko, The extended/generalized finite element method: An overview of the method and its applications, *International Journal for Numerical Methods in Engineering* 84 (3) (2010) 253–304.
- [14] T. Belytschko, S. P. Xiao, C. Parimi, Topology optimization with implicit functions and regularization, *International Journal for Numerical Methods in Engineering* 57 (8) (2003) 1177–1196.
- [15] L. Van Miegroet, P. Duysinx, Stress concentration minimization of 2D filets using X-FEM and level set description, *Structural and Multidisciplinary Optimization* 33 (4-5) (2007) 425–438.
- [16] P. Wei, M. Y. Wang, X. Xing, A study on X-FEM in continuum structural optimization using a level set model, *Comput-Aided Design* 42 (8) (2010) 708–719.
- [17] S. Ha, S. Cho, Level set based topological shape optimization of geometrically nonlinear structures using unstructured mesh, *Computers and Structures* 86 (13–14) (2008) 1447–1455.

- [18] S. Yamasaki, T. Nomura, A. Kawamoto, K. Sato, S. Nishiwaki, A level set-based topology optimization method targeting metallic waveguide design problems, *International Journal for Numerical Methods in Engineering* 87 (9) (2011) 844–868.
- [19] S. Yamasaki, S. Nishiwaki, T. Yamada, K. Izui, M. Yoshimura, A structural optimization method based on the level set method using a new geometry-based re-initialization scheme, *International Journal for Numerical Methods in Engineering* 83 (12) (2010) 1580–1624.
- [20] K. Abe, S. Kazama, K. Koro, A boundary element approach for topology optimization problem using the level set method, *Communications in Numerical Methods in Engineering* 23 (5) (2007) 405–416.
- [21] K. Abe, T. Fujiu, K. Koro, A be-based shape optimization method enhanced by topological derivative for sound scattering problems, *Engineering Analysis with Boundary Elements* 34 (12) (2010) 1082–1091.
- [22] G. Allaire, F. Jouve, A level-set method for vibration and multiple loads structural optimization, *Computer Methods in Applied Mechanics and Engineering* 194 (3033) (2005) 3269–3290.
- [23] H. Jia, H. Beom, Y. Wang, S. Lin, B. Liu, Evolutionary level set method for structural topology optimization, *Computers and Structures* 89 (5-6) (2011) 445–454.
- [24] P. D. Dunning, H. A. Kim, A new hole insertion method for level set based structural topology optimization, *International Journal for Numerical Methods in Engineering* 93 (1) (2013) 118–134.
- [25] X. Huang, Y. M. Xie, *Evolutionary Topology Optimization of Continuum Structures: Methods and Applications*, New York: John Wiley & Sons, 2010.
- [26] Q. Li, G. P. Steven, Y. M. Xie, On equivalence between stress criterion and stiffness criterion in evolutionary structural optimization, *Structural Optimization* 18 (1) (1999) 67–73.
- [27] B. Ullah, J. Trevelyan, P. Matthews, Structural optimisation based on the boundary element and level set methods, *Computers & Structures* 137 (2014) 14–30.

- [28] B. Ullah, J. Trevelyan, Correlation between hole insertion criteria in a boundary element and level set based topology optimisation method, *Engineering Analysis with Boundary Elements* 37 (11) (2013) 1457–1470.
- [29] J. A. Sethian, *Level Set Methods and Fast Marching Methods: Evolving Interfaces in Computational Geometry, Fluid Mechanics, Computer Vision, and Materials Science*, 2nd Edition, Cambridge University Press, 1999.
- [30] O. M. Querin, G. P. Steven, Y. M. Xie, Evolutionary structural optimisation (ESO) using a bidirectional algorithm, *Engineering Computations* 15 (8) (1998) 1031–1048.
- [31] G. P. Steven, , L. Qing, K. Proos, Y. M. Xie, The role of physical sensitivity in evolutionary topology design optimisation with multi-criteria and multi-physics, in: *Proceedings of Fifth World Congress on Computational Mechanics (WCCM V)*. Vienna, Austria., 2002.
- [32] E. Cervera, J. Trevelyan, Evolutionary structural optimisation based on boundary representation of NURBS. Part I: 2D algorithms, *Computers and Structures* 83 (2005) 1917–1929.
- [33] E. Cervera, J. Trevelyan, Evolutionary structural optimisation based on boundary representation of NURBS. Part II: 3D algorithms, *Computers and Structures* 83 (2005) 1902–1916.
- [34] J. Li, P. Agathoklis, An efficiency enhanced isosurface generation algorithm for volume visualization, *The Visual Computer* 13 (9-10) (1998) 391–400.
- [35] W. E. Lorensen, H. E. Cline, Marching cubes: A high resolution 3d surface construction algorithm, *Computer Graphics* 21 (4) (1987) 163–169.
- [36] T. S. Newman, H. Yi, A survey of the marching cubes algorithm, *Computers and Graphics* 30 (5) (2006) 854–879.
- [37] R. Bade, J. Haase, B. Preim, Comparison of fundamental mesh smoothing algorithms for medical surface models, in: *Simulations and Visualisierung*, Vol. 6, 2006, pp. 289–304.

- [38] B. H. V. Topping, J. Muylle, P. Ivanyi, Finite element mesh generation, Saxe-Coburg publications on computational engineering, Saxe-Coburg Publications, Stirling, Scotland, 2004.
- [39] T. M. Foster, M. S. Mohamed, J. Trevelyan, G. Coates, Rapid re-meshing and re-resolution of three-dimensional boundary element problems for interactive stress analysis, *Engineering Analysis with Boundary Elements* 36 (9) (2012) 1331–1343.
- [40] J. Vollmer, R. Mencl, H. Mueller, Improved laplacian smoothing of noisy surface meshes, in: *Computer Graphics Forum*, Vol. 18, Wiley Online Library, 1999, pp. 131–138.
- [41] A. A. Becker, *The Boundary Element Methods in Engineering: A complete course*, McGRAW - HILL BOOK COMPANY, 1992.
- [42] D. Adalsteinsson, J. A. Sethian, The fast construction of extension velocities in level set methods, *Journal of Computational Physics* 148 (1) (1999) 2–22.
- [43] D. Adalsteinsson, J. A. Sethian, A fast level set method for propagating interfaces, *Journal of Computational Physics* 118 (2) (1995) 269–277.
- [44] J. C ea, S. Garreau, P. Guillaume, M. Masmoudi, The shape and topological optimizations connection, *Computer Methods in Applied Mechanics and Engineering* 188 (4) (2000) 713–726.
- [45] X. Huang, Y. M. Xie, Convergent and mesh-independent solutions for the bi-directional evolutionary structural optimization method, *Finite Elements in Analysis and Design* 43 (14) (2007) 1039–1049.
- [46] C. Bertsch, A. P. Cisilino, N. Calvo, Topology optimization of three-dimensional load-bearing structures using boundary elements, *Advances in Engineering Software* 41 (5) (2010) 694–704.
- [47] A. A. Novotny, R. A. Feij oo, E. Taroco, C. Padra, Topological sensitivity analysis for three-dimensional linear elasticity problem, *Computer Methods in Applied Mechanics and Engineering* 196 (41) (2007) 4354–4364.

- [48] O. Sigmund, A 99 line topology optimization code written in Matlab, *Structural and Multidisciplinary Optimization* 21 (2) (2001) 120–127.
- [49] J. B. Jacobsen, N. Olhoff, E. Rønholt, Generalized shape optimization of three-dimensional structures using materials with optimum microstructures, *Mechanics of Materials* 28 (1998) 207–225.
- [50] V. Young, O. M. Querin, G. P. Steven, Y. M. Xie, 3D and multiple load case bi-directional evolutionary optimization (BESO), *Structural Optimization* 18 (1999) 183–192.
- [51] G. Allaire, C. Dapogny, P. Frey, Shape optimization with a level set based mesh evolution method, *Computer Methods in Applied Mechanics and Engineering* 282 (2014) 22–53.